CENTRO FEDERAL DE EDUCAÇÃO TECNÓLOGICA DE MINAS GERAIS
Diretoria de Pesquisa e Pós-Graduação
Programa de Pós-Graduação em Engenharia Mecânica

MASTER's THESIS

ALEX HENRIQUE COUTINHO SANTOS

AIR CONDITIONING SYSTEM INTEGRATED WITH THERMAL ENERGY STORAGE FOR BUILDINGS

Belo Horizonte
2023

Alex Henrique Coutinho Santos

AIR CONDITIONING SYSTEM INTEGRATED WITH THERMAL ENERGY STORAGE FOR BUILDINGS.

Dissertation presented to the Postgraduate Program in Mechanical Engineering of the Centro Federal de Educação Tecnológica de Minas Gerais as a partial requirement for obtaining the title of Master in Mechanical Engineering.

Advisor: Prof. Dr. Tiago de Freitas Paulino

Co-advisor: Prof. Dr. Willian Moreira Duarte

Research Field: Energy Efficiency

Belo Horizonte
2023

Santos, Alex Henrique Coutinho
S237a Air conditioning system integrated with thermal energy storage for buildings / Alex Henrique Coutinho Santos . – 2023.
73 f. : il., gráfs, tabs.

Dissertação apresentada ao Programa de Pós-Graduação em Engenharia Mecânica do Centro Federal de Educação Tecnológica de Minas Gerais.
Orientador: Tiago de Freitas Paulino.
Coorientador: Willian Moreira Duarte.
Banca examinadora: Tiago de Freitas Paulino, Willian Moreira Duarte, Paulo Eduardo Lopes Barbieri e Luiz Machado.
Bibliografia: f. 68-73.
Dissertação (mestrado) – Centro Federal de Educação Tecnológica de Minas Gerais.

1. Ar condicionado – Modelos matemáticos – Teses. 2. Calor – Armazenamento – Teses. 3. Materiais – Propriedades termais – Teses. I. Paulino, Tiago de Freitas. II. Duarte, Willian Moreira. III. Centro Federal de Educação Tecnológica de Minas Gerais. IV. Título.

CDD 697.93

Elaboração da ficha catalográfica pela bibliotecária Jane Marangon Duarte, CRB 6º 1592 / Cefet/MG

Alex Henrique Coutinho Santos

AIR CONDITIONING SYSTEM INTEGRATED WITH THERMAL ENERGY STORAGE FOR BUILDINGS.

Dissertation presented to the Postgraduate Program in Mechanical Engineering of the Centro Federal de Educação Tecnológica de Minas Gerais as a partial requirement for obtaining the title of Master's in Mechanical Engineering.

Research Field: Energy Efficiency

Belo Horizonte, November 27th, 2023

Result: Approved

Examining Board:

Prof. Dr. Tiago de Freitas Paulino (Advisor)

Centro Federal de Educação Tecnológica de Minas Gerais

Prof. Dr. Willian Moreira Duarte (Co-advisor)

Universidade Federal de Minas Gerais

Prof. Dr. Paulo Eduardo Lopes Barbieri

Centro Federal de Educação Tecnológica de Minas Gerais

Prof. Dr. Luiz Machado

Universidade Federal de Minas Gerais

DEDICATION

I dedicate this work to my wife, Bárbara, to my children, Catarina and Tereza, and my parents, Cláudio and Gildete, for all the support provided during the development of this work.

ACKNOWLEDGMENTS

This study was partially funded by the Coordenação de Aperfeiçoamento de Pessoal de Nível Superior - Brasil (CAPES) - Financial Code 001, this work was supported by the Fundação de Amparo à Pesquisa do Estado de Minas Gerais (FAPEMIG), Conselho Nacional de Desenvolvimento Científico e Tecnológico (CNPq), through scientific initiation grants.

I would like to express my gratitude to the post-graduate programme in mechanical engineering at CEFET.

ABSTRACT

Thermal Energy Storage (TES) is an innovative technology that can help mitigate environmental problems and make energy consumption in air-conditioning systems more efficient. TES also helps to decouple the production and use of cooling. In this work, a mathematical model was developed to obtain the thermal loads of the environment based on Brazilian standards and to simulate the operation of an air-conditioning system integrated with TES. A refrigeration system that provides cooling capacity for the selected environment was used to simulate simulates the operation of refrigeration systems to evaluate the coefficient of performance of the refrigeration cycle and the refrigeration system, including the TES, during the days 23.01.2019 (maximum sum of solar radiation), 17.05.2019 (day with a lower maximum temperature) and 20.12.2019 (maximum annual temperature) for the city of Teresina, in the Northeast region of Brazil. On each day, the efficiency of the refrigerant R134a was verified. Based on the data obtained from the mathematical simulation model, a thermal impact analysis was carried out for Brazil. The reduction in energy consumption varies between 9.4% and 1.3%.

Keywords: Mathematical model. Air conditioning system. Thermal Energy Storage. Phase Change Materials.

RESUMO

SISTEMA DE AR-CONDICIONADO INTEGRADO COM ARMAZENAMENTO DE ENERGIA TÉRMICA PARA EDIFÍCIOS

O Armazenamento de Energia Térmica (TES) é uma tecnologia inovadora que pode ajudar a mitigar problemas ambientais e tornar mais eficiente o consumo de energia em sistemas de ar-condicionado. O TES também ajuda a dissociar a produção e o consumo nos sistemas de refrigeração. Neste trabalho foi desenvolvido um modelo matemático para obter as cargas térmicas do ambiente com base nas normas brasileiras e para simular o funcionamento de um sistema de ar-condicionado integrado ao TES. É utilizado um sistema de refrigeração capaz de fornecer capacidade de refrigeração para o ambiente selecionado. Ele simula o funcionamento de sistemas de refrigeração para avaliar o coeficiente de desempenho do ciclo de refrigeração e do sistema de refrigeração, incluindo o TES, durante os dias 23.01.2019 (dia com a soma máxima de radiação solar), 17.05.2019 (dia com menor temperatura máxima) e 20.12.2019 (temperatura máxima anual) para a cidade de Teresina, região Nordeste do Brasil. Em cada dia é verificada a eficiência do refrigerante R134a. Com base nos dados obtidos no modelo de simulação matemática, foi realizada uma análise de impacto térmico. A redução no consumo de energia varia entre 9,4% e 1,3%

Palavras-chave: Modelo matemático. Sistema de ar-condicionado. Reservatório de energia térmica. Materiais com mudança de fase.

LIST OF FIGURES

LIST OF TABLES

LIST OF ABBREVIATIONS

ABNT Associação Brasileira de Normas Técnicas

COP Coefficient of Performance

CEFET-MG Centro Federal de Educação Tecnológica de Minas Gerais

COP_G Coefficient of Performance global

COP_R Coefficient of Performance of the refrigeration system

EG Ethylene Glycol

EPE The Brazilian Energy Research Enterprise (Empresa Brasileira de Pesquisas Energéticas)

HTF Heat Transfer Fluid

HVAC Heating, Ventilating and Air Conditioning

HVAC&R Heating, Ventilation, Air Conditioning, and Refrigeration

NBR Brazilian Standard (Norma brasileira)

PI Piauí State

PCC Phase Change Composite

PCM Phase Change Material

PPGEM Postgraduate Program in Mechanical Engineering (Programa de Pós-graduação em Engenharia Mecânica)

PROCEL National Electric Energy Conservation Program (Programa Nacional de Conservação de Energia Elétrica)

TES Thermal Energy Storage

UFMG Universidade Federal de Minas Gerais

LIST OF NOMENCLATURE

Special symbols

a_m	PCM melted fraction [%]
ΔH	Difference of latent heat [kJ/kg]
ΔT	Temperature difference [K]
F_a	Air renewal factor per area [(m³/s)/m²]
F_{per}	Air renewal factor per person [(m³/s)/person]
F_{s_c}	Roof solar factor
F_{s_p}	Wall solar factor
$\bar{h}$	Average convective coefficient [W/(m² K)]
$\dot{m}$	Mass flow rate [kg/s]
$\dot{Q}$	Heat transfer rate [W]
$\dot{Q}_{arr}$	Air renewal rate [W]
$\dot{Q}_{cht}$	Heat transfer by conduction [W]
$\dot{Q}_e$	Hourly thermal load [W]
$\dot{Q}_{ele}$	Heat transfer rate by equipment [W]
$\dot{W}$	Power [W]

Latin symbols

A	Cross-section area [m²]
C	Heat capacity at constant pressure [J/(kg . K)]
Cp	Specific heat at constant pressure [kJ/kg . K]

D	Diameter of tube [m]
F	Energy generated per person [W]
H	Room height [m]
I	Hourly solar radiation
i	Specific enthalpy [J/kg]
Ilu	Thermal load generated by lighting [W/m²]
k_C	Thermal conductivity of material of refrigerant tube in the condenser [W/(m.K)]
L	Length of tube [m]
Le	Room length [m]
m	Mass [kg]
N	Rotation speed [1/s]
Np	Number of people
NTU	Number of transfer units
P	Pressure [Pa]
Q	Amount of energy stored in PCM [J]
r	Pressure ratio
s	Entropy [J/K]
T	Temperature[K]
time	Actual time
UA	Condenser global heat transfer coefficient [W/(m² K)]
V	Compressor displacement volume [m³]
W	Room Width [m]

Greek and special symbols

ρ Specific mass [kg/m³]

η Efficiency [%]

π Pi

v Specific volume [m³/kg]

ζ Heat leakage coefficient

φ Thermal delay

Common subscripts

1 Compressor inlet

2 Air condenser inlet

3 Expansion device inlet

4 Evaporator inlet

air Air

C Ceiling

$Comp$ Compressor

$Cond$ Condenser

ED Expansion device

ev Evaporator

ext External

f Final

F Floor

i inicial

i	Inlet
ii	Inner diameter of inner tube
int	Internal
L	Liquid state
lig	Lighting
m	Melting
max	Maximum
oi	Outer diameter of inner tube
o	Outlet
P	Pump
PCM	Phase Change Material properties
per	Person
ref	Refrigerant
S	Solid state
sun	Sun
$total$	Total
v	Volumetric
W	Water
Wa	Walls

SUMMARY

1 INTRODUCTION

Although significant efforts have been made, climate change continues to pose a major challenge. It is also crucial to reduce greenhouse gas emissions in the residential sector. In 2021, households are expected to account for 27.4% of final energy consumption in the European Union, with 77.8% of residential energy consumption used for space heating and hot water. Consequently, there is a growing interest in developing energy-efficient and sustainable solutions for space heating and hot water applications (KUTLU *et al.*, 2023).

In recent decades, power companies have observed a transition in electricity demand patterns. Peak energy demand growth has outpaced overall electricity demand growth, resulting in lower load factors. This makes it increasingly difficult for concessionaires to plan for the short and long term. The transition in consumption patterns translates into a less efficient system, which increases the overall operating costs of the electrical system. Furthermore, the aging infrastructure of the current power distribution system with limited capacity is also a concern due to increasing energy demand (PALACIO*et al.*, 2014).

The generation of energy from fossil fuels is currently the primary source of global energy (IEA, 2021); global warming was recognized worldwide through the Kyoto Protocol in 1997, which resulted in a global commitment to reduce greenhouse gas emissions. It is important to note that anthropogenic CO2 is not the only cause of global warming. In December 2015, the Paris Agreement introduced measures to limit the global average temperature rise to below 2°C above pre-industrial levels (REAL-FERNÁNDEZ *et al.*, 2019).

Society's energy demands are increasing, while resources dominating most national energy systems are limited and predicted to become scarcer and more expensive in the coming years (ABEDIN and ROSEN, 2011). Although renewable resources have great energy potential, they are not always fully accessible and can be regional, seasonal, and intermittent (NKWETTA and HAGHIGHAT, 2014).

In regions with extreme weather conditions, there are large variations in the supply and consumption of energy related to the need for domestic hot water and the application of space heating and/or cooling due to the large thermal amplitude and seasonality. Changing energy supply and consumption results in peak and off-peak energy usage, leading to the surcharge of energy prices offered during peak energy demand compared to peak energy demand (NKWETTA and HAGHIGHAT, 2014).

In 2017, electrical air conditioning systems represented the consumption of 17% of the total electrical energy consumed in Brazilian homes (EPE , 2018); in addition, there is a study that indicates that electrical air conditioning systems may account for 85% of the consumption of residential electric energy in the peak of summer (LI, LIU and WANG, 2019) and in commercial establishments approximately 40% of the electric energy consumed is destined for the acclimatization of environments (PROCEL, 2008). An innovative technology that can collaborate to mitigate environmental problems and make energy consumption more efficient and that has wide applications is thermal energy storage (TES).

The refrigeration process is one of the biggest energy consumers; the cold storage TES is composed of a process in which cold energy is loaded into the material in the medium in the charging process and then extracted in the process of discharging this energy when necessary. During the TES loading process, the cold is accumulated in the phase change material (PCM), and then the available cold is extracted when necessary (VEERAKUMAR and SREEKUMAR, 2016).

The use of thermal energy storage (TES) in industrial and residential installations is continuously growing, as is the increase in electrical energy consumption. The use of TES has two main points. First, it allows for the rationalization of power supply capacity, as TES can reduce demand during peak hours once the cold energy can be produced during the night or when the environmental conditions are more favourable. The second important point is the balance of consumption in situations with a time lag between supply and consumption (ALLOUCHE *et al.*, 2015). Cold can be stored due to internal energy properties or phase change of the material stored in the TES. The system can be applied to reduce energy consumption; the cold load is generated and stored for peak energy consumption times.

1.1 - Objectives

The aim objective of this investigation was to develop a mathematical model that can obtain the thermal loads of an environment and simulate the operation of an air conditioning system integrated with thermal energy storage.

1.1.1 Specific objectives

- Implement mathematical modelling for energy storage in a material with phase change;
- Implement mathematical model to obtain thermal loads;

- Implement a mathematical model for the climatization system;
- Coupling the models and establishing simulation conditions that enable thermal impact analysis for a city in Brazil.

1.2 - Outline of the Master thesis

This Master thesis is divided into the following five chapters:

- Chapter 1 states the motivation and background for this work as well as the objectives;
- Chapter 2 contains a review of the literature and describes relevant scientific works that have a direct relation with the theme of this master thesis;
- Chapter 3 describes the methods used in this master thesis;
- Chapter 4 presents the results of this investigation;
- Chapter 5 provides conclusions.

The contributions of the master's thesis are linked to the papers listed in Annex I.

2 LITERATURE REVIEW

Thermal energy storage (TES) is one of the most applied methods for accumulating thermal energy and shifting electricity consumption from peak load moments. The advantages of TES systems over chemical-based technologies are the installation and maintenance costs and the reduction of environmental impacts. TES allows the storage of extra thermal energy to be used for future consumption, with this being possible to balance demand and consumption between day and night, for example (AJAROSTAGHI *et al.*, 2019).

The advantage of using TES in an HVAC system is that it increases the system's overall efficiency, improves reliability, and can generate savings in running costs and less pollution of the environment. Photovoltaic energy systems with great efficiency are mature and applied industrial and use a large part of the sun's thermal energy during the day. However, they do not have enough backup to continue their operation during low or no solar radiation (SARBU and SEBARCHIEVICI, 2018).

Thermal energy storage could be defined as the temporary holding of thermal energy for later utilization (ABEDIN and ROSEN, 2011). The energy demands vary daily, weekly, and in seasons; these demands can be minimized with the TES systems once it is possible to store energy by cooling, heating, melting, solidifying, or vaporizing a Phase Change Material (PCM) and the thermal energy becomes available when the process is reversed. TES can become a conventional system more efficiently, particularly by bridging the period between when energy is harvested and when it is needed (SOCACIU, 2012). The main types of TES are:

- Sensible TES: they are composed of materials that store energy by changing the environment's temperature; temperature variation and the quantity of the material are the main factors that determine the amount of energy storage capacity. Those systems can be filled with water, stones, sand, soil, etc.
- Latent TES: They are composed of materials that change the amount of energy stored through a phase from one state to another (e.g., solid to liquid), PCM. Those systems can be filled with water/ice, paraffin, etc.

This characteristic is determined by the material stored. TES could be used to balance the supply and demand of energy in your system, becoming more effective and cheaper by bridging the period between when energy is harvested and when it is needed. Storage capacity with small temperature variations and irrelevant volume changes are the main characteristics of PCMs. Those features allow them to be implemented in buildings for thermal management (AKEIBER *et al.*, 2016).

The complete cycle of a TES involves at least three phases: charging, storage, and discharging of thermal energy. During an operating cycle, one or more steps occur simultaneously; sometimes, the same step can occur more than once during one cycle.

Latent TES is one of the most efficient ways of accumulating energy (SOCACIU, 2012) since the accumulation is performed during the material's phase change (melting, evaporating, crystallization). Due to the specific heat of the material used in the TES, the difference in enthalpy during the phase change and the change in latent heat is generally greater than the change in sensitive heat for a given material in each size system. The latent heat storage method offers a greater amount of storage with a smaller temperature difference between the loading and unloading phases of the system when compared to the sensitive heat (DUTRA, DUARTE and PAULINO, 2020).

2.1 - Phase Change Material (PCM)

Thermal energy can be stored as sensible heat, latent heat, or chemical reactions. Phase change materials (PCMs) are included in the second storage mechanism as they harness latent heat from the freezing and melting processes (PARDIÑAS *et al.*, 2017). PCM can undergo three types of phase change: solid-solid, solid-liquid, and liquid-gas. Solid-to-solid transition generally occurs at high transition temperatures, far beyond practical applications. Liquid-gas transitions are not considered for most applications due to the large volume variation associated with their phase transition. Solid-liquid transitions, however, have many applications as they have high latent heat capacities, making them viable for various applications (XIA *et al.*, 2014). Phase change materials can be divided into three groups:

- Organic PCM: organic phase change materials are, in general, chemically stable, do not suffer from supercooling, are non-corrosive, are non-toxic, and have a high latent heat of fusion (BAETENS, JELLE and GUSTAVSEN, 2010). They cover a range of melting points between 0°C and 200°C. Most of them are unstable at high temperatures because of their high levels of carbon and hydrogen. The densities of organic PCMs are commonly lower than 1 g/cm³ and usually have smaller heats of fusion per volume than inorganic PCMs (XIA *et al.*, 2014).
- Inorganic PCM: inorganic PCMs often have mass melting enthalpies similar to organic PCMs but higher by volume due to their high densities, good thermal

conductivity, sharp melting points, and non-flammability. However, most are corrosive to most metals, undergo supercooling, and undergo phase decomposition.

- Eutectic PCM: eutectic PCM is a mixture of various solids in such proportions that the melting point is as low as possible, usually has sharp melting points, and the density is slightly higher than that of organic compounds (BAETENS, JELLE and GUSTAVSEN, 2010).

The vast majority of latent TES are composed of PCMs with thermal energy storage in the material's phase change, commonly from solid to liquid; the amount of energy stored is based on the latent heat of fusion of the material PCM (SOCACIU, 2012). Some thermo-physical, kinetic, and chemical properties of a material are desirable for use as a PCM, which is listed below (VEERAKUMAR and SREEKUMAR, 2016).

- The melting temperature of the PCM should be in the range of operating temperature;
- High Latent heat of fusion;
- High thermal conductivity;
- High density;
- Low volume change during phase change;
- Less corrosive to the construction materials;
- Low degradation;
- Chemically stable;
- Non-toxic and non-flammable;
- Easily available;
- Cost-effective.

2.2 - Refrigeration cycle with TES

Evaluating recent studies of the application of TES with air conditioning systems, it can be noted that the choice of PCM must be made considering the material's ability to store the cold energy and discharge it when necessary. That choice must be guided according to the location where the system will be installed, such as thermal amplitude. Different researchers were developed to evaluate PCM with a focus on its application in air conditioning systems to enhance performance and save energy, making consumption more linear once the usage of TES dissolves the peak time during the day.

AL-ABIDI *et al.*, 2013 investigate the application of TES composed of a triplex tube heat exchanger with a PCM in the middle of the tube, as shown in **Figure 1**. The experiment evaluated the effects of mass flow rates and heating methods on PCM melting process. It investigated three techniques (heating the inside tube, heating the outside tube, and heating both sides). They analysed the gradients of PCM temperature in the radial, angular, and axial directions PCM temperature. Three heating methods investigated PCM melting in the TES middle tube; in the first case, PCM melting was not completed within the required time, whereas in the second and third cases, complete PCM melting was achieved within less than the required time. As the flow rate increased, the average temperature of the PCM increased, and a shorter time was required for the PCM to melt. A variation in the temperature was observed in the radial and angular directions, whereas no significant variation in the axial direction was observed.

Figure 1 - Schematic diagrams of experimental apparatus

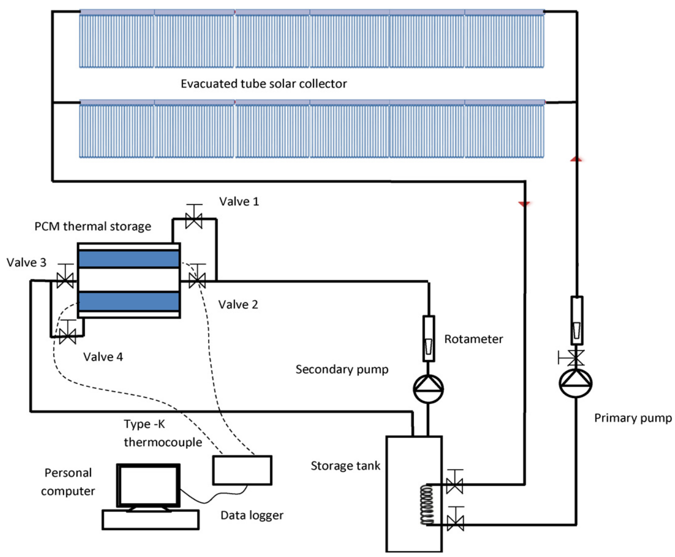

Source: AL-ABIDI *et al.*, 2013

FASL *et al.*, 2014 developed and implemented a model using the MATLAB/Simulink framework where a hybrid system (conventional system and HVAC&R with an active TES unit) with an appropriate thermal control to increase the efficiency of an HVAC system as shown in **Figure 2**. The results indicated that the space achieved the desired temperature 62% faster for the hybrid system and with a COP 11.1% higher than the conventional system.

Figure 2 - Hybrid thermal system schema

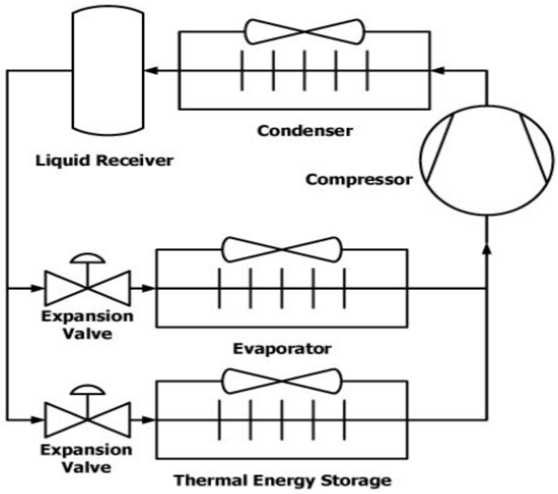

Source: FASL *et al.*, 2014

CHAIYAT, 2015 studied the concept of using PCM to improve the air conditioning system's efficiency. In his study, the selected PCM was RT-20, which was packed in balls, as presented in **Figure 3**, to evaluate the air conditioning system's thermal performance, reducing the air temperature at the evaporating coil's entrance. To reduce the temperature, he made a bed of balls 40 cm thick, and the mathematical model was developed and verified with testing results. The results were compared to the mathematical model, which agreed quite well with the experimental results; the model was applied for the economic analysis, where he concluded the air conditioning system with PCM could save 9.10% of electrical power costs, and the payback period was around 4.15 years.

ZHAO and TAN, 2015 proposed integrating a shell-and-tube TES with a conventional air conditioning system to increase the performance, the TES functions as a heat sink to the air-conditioner during the daytime cooling period. At night, the heat stored in the PCM will be discharged using relatively cool outdoor air. The shell-and-tube TES uses two different media (water and air) as heat transfer fluid (HTF). For the HTF, water was used for the charging loop, while air was used for the discharging loop, as shown in **Figure 4**. This study developed a numerical model for TES unit, considering the effects of natural convection in the melting process of the PCM.

Figure 3 - Prototype of the air conditioning integrating system

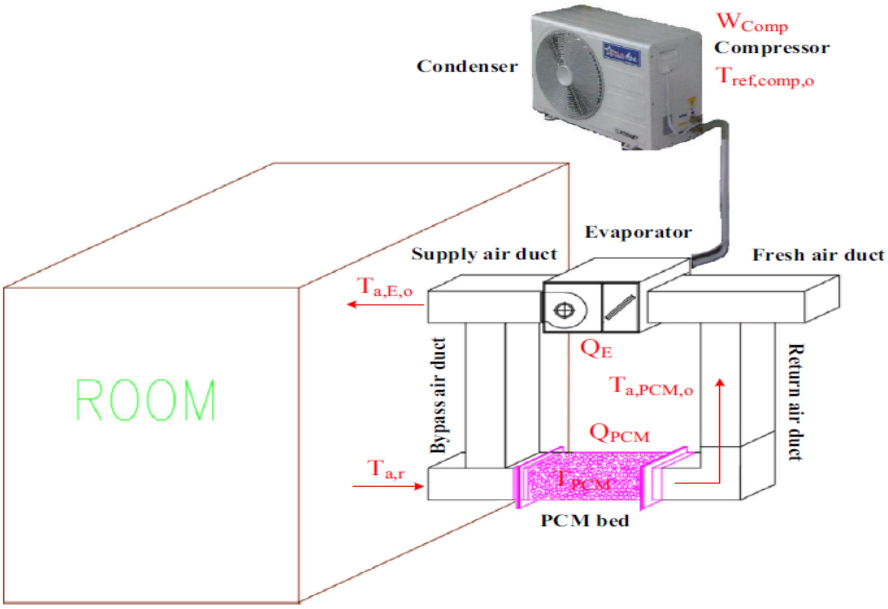

Source: CHAIYAT, 2015

The numerical study evaluated the effects of HTF inlet temperature, flow rate, and conductive fin height on the TES system performance. In the heat charging process of the proposed TES, higher HTF inlet temperature, mass flow rate, and fin height provide a higher TES charging rate and shorter total charging time. Numerical modelling was used to find the optimum fin height to balance PCM thermal storage system's performance and cost. The effectiveness of this proposed TES system is generally higher than 0.5. The proposed case for replacing the conventional cooling tower using the proposed TES system for a water-cooled air-conditioner shows a COP value increase of about 25.6%.

Figure 4 - Schematic diagram of air conditioning integrated with TES

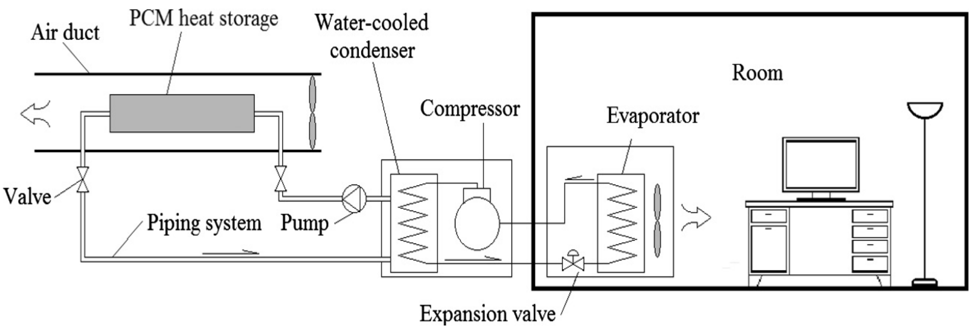

Source: ZHAO and TAN, 2015

SAID and HASSAN, 2018 presented a study of implementing a new technique that uses a TES integrated with a conventional air conditioning system to increase its cooling performance. His technique is based on integrating TES plates to cool fresh air at the air conditioning unit's condenser, as shown in **Figure 5**. The PCM inside the plates stores cold during the night-time and charging period and uses its cold during the daytime to refresh the air at the inlet of the air conditioning unit's condenser during the discharge period. He proposed a theoretical transient model for the PCM with an air heat exchanger, and the results of this mathematical model were validated with experimental data. The work evaluated the effects of plate configurations, inlet air flow rate, temperature of the inlet air in the process of charge and discharge of the TES, and the air conditioning system's performance. The study concludes that for the same cross-section area of the plates, the melting time, cooling time, solidification time, and outlet air temperature are decreased with decreasing plate width and increasing length. Increasing the velocity and temperature of the air inlet to the PCM plates increase the outlet air temperature. The coefficient of performance of the air conditioning unit, the useful cooling power of the phase change material plates, and saved power decrease the cooling time. His work shows the best performance enhancement is 14%, depending on the characteristics (width, length) of your system.

Figure 5 – Model of air conditioning with TES

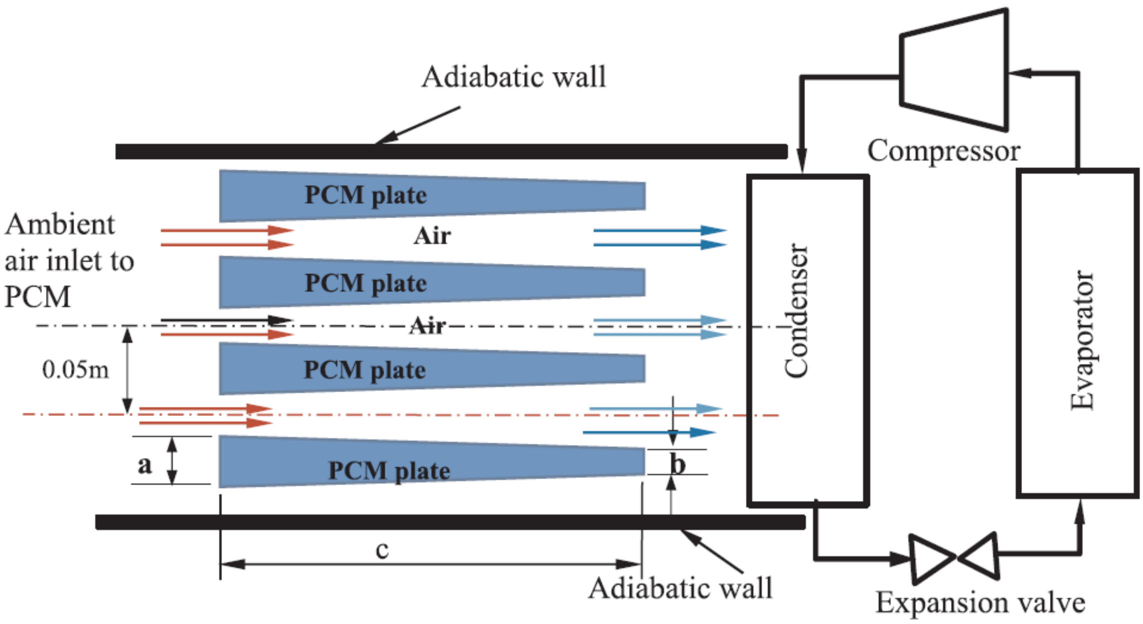

Source: SAID and HASSAN, 2018

LI *et al.*, 2018 to improve TES system performance, proposed a multiple-PCM-based TES unit for use in conventional air conditioning systems, as shown **Figure 6**. Three PCMs (PCM-1, PCM-2, and PCM-3) with phase change temperatures of 5.3 °C, 6.5 °C and 10 °C, respectively, were used. They studied the application of three PCMs with different phase change temperatures. Water was used as HTF. They proposed a model developed in ANSYS FLUENT to investigate the charging process, and to validate the model, an experimental system was constructed. The simulation indicates that an increase of approximately 32.22%

of cold energy occurs in the multiple-PCM system compared to a system with a single PCM, while the charging time of TES becomes shorter.

Figure 6 - Schematic diagram of the experimental apparatus

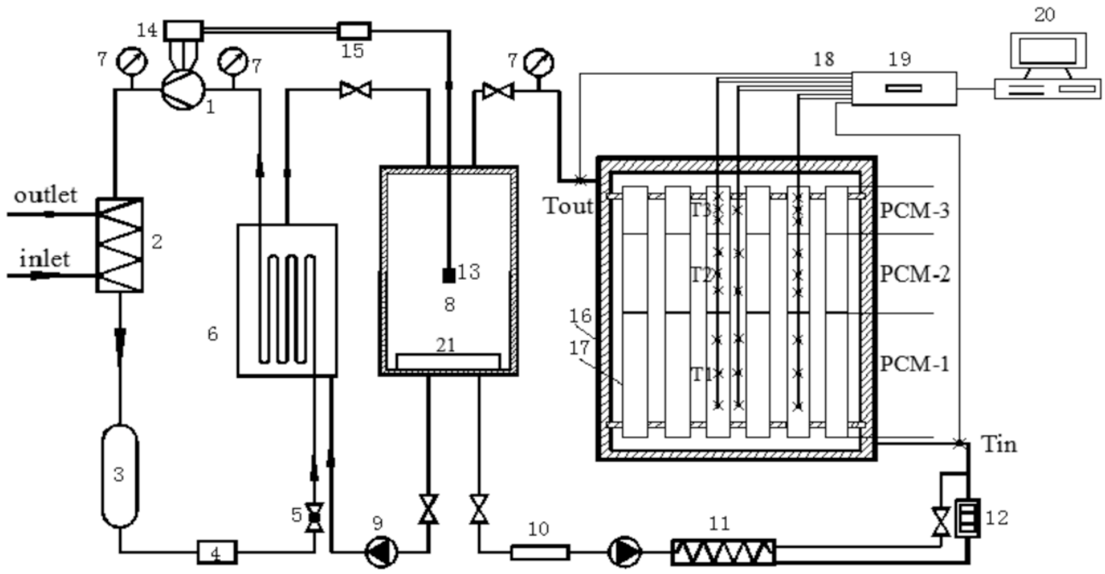

Source: LI *et al.*, 2018

AJAROSTAGHI *et al.*, 2019 developed a numerical model for a three-dimensional study using ANSYS Fluent to verify the efficiency of a system with a tube and shell, as shown in **Figure 7**. An internal coil was dipped into ice as PCM evaluated the influence of dynamic parameters: inlet temperature and refrigerant flow rate. In addition, geometrical parameters, such as coil pitch, diameter, and height, are analysed in the PCM melting process. Results indicate, for all geometric parameters analysed, that increasing the HTF inlet temperature leads to a reduction of the melting time in order of 23 – 33%, while increasing the mass flow rate decreases the melting time in order of 2%. Regarding the geometrical influence, the coil diameter exhibits the most significant effect on the melting rate.

Figure 7 - Schematic of shell and coil tube TES with relevant geometrical parameters

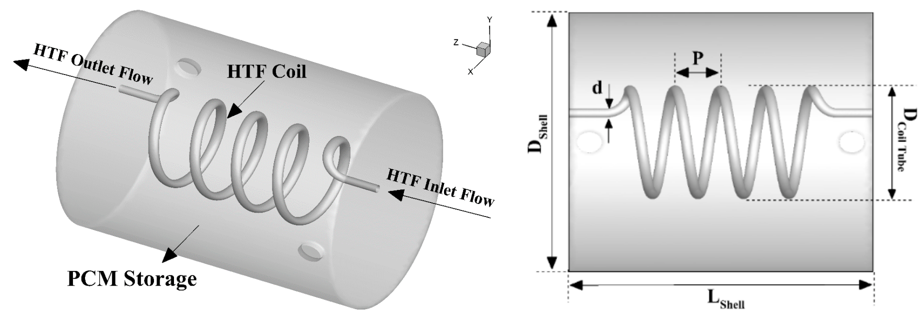

Source: AJAROSTAGHI *et al.*, 2019

SAID and HASSAN, 2019 studied a TES coupled with an air conditioning system, as shown in **Figure 8**. The TES charges at night, and the accumulated energy is used during the day. The performance was evaluated during the charging and discharging of the TES in different inlet ambient air temperatures and velocities. The developed mathematical model was solved using ANSYS Fluent software. The results demonstrate that during the discharging process, the outlet air temperature from the PCM plates is reduced by increasing the inlet air temperature and velocity. The rate of PCM melting increases with increasing the ambient temperature; decreasing the PCM plate width has the advantage of reducing the solidification time, but it reduces the saving power by about 10.5%.

Figure 8 - Model of the PCM unit with air conditioning

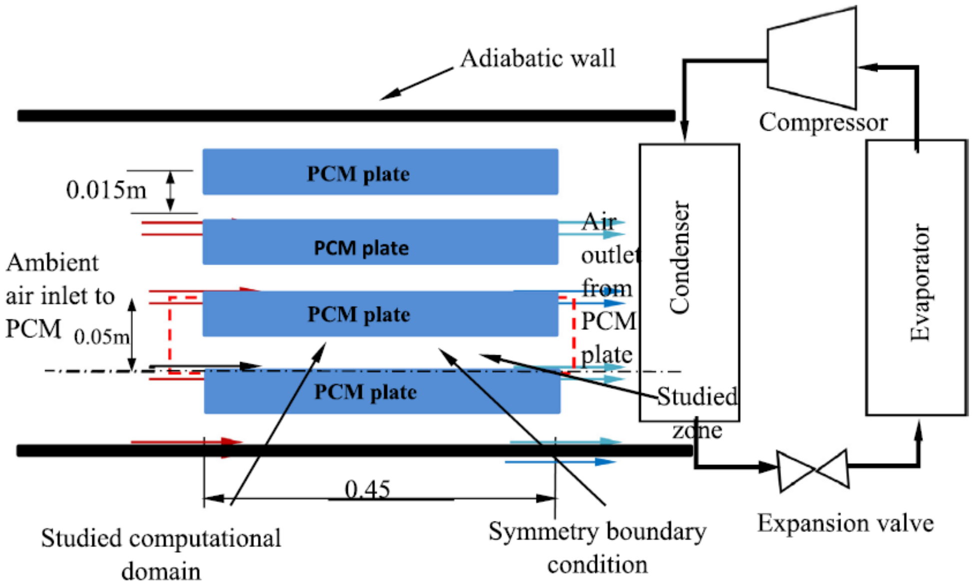

Source: SAID and HASSAN, 2019

ALJEHANI, NITSCHE and AL-HALLAJ, 2020 present in his theoretical study a detailed numerical analysis to describe the heat transfer transient in a TES with a Phase Change Composite material (PCC), composed of 78% low-temperature paraffin, namely n-Tetradecane (C14H30) and 22% expanded graphite, exchanging heat with the refrigerant fluid of the refrigeration system. **Figure 9** presents the proposal made for a hybrid refrigeration system, where the TES system works in parallel to the refrigeration system. Ethylene Glycol (EG) loop #1 mediates heat exchange between incoming hot air and the PCC during the discharging time during peak demand times, and Ethylene Glycol (EG) loop #2 mediates heat exchange between the refrigerant and the PCC during charging time night. Results were validated using experimental data; the variations between the experimental and theoretical model were approximately (4 – 9%) and attributed to the heat loss in the actual experiment, which demonstrated acceptable agreement and an accurate representation.

Figure 9 - Schematic block flow diagram

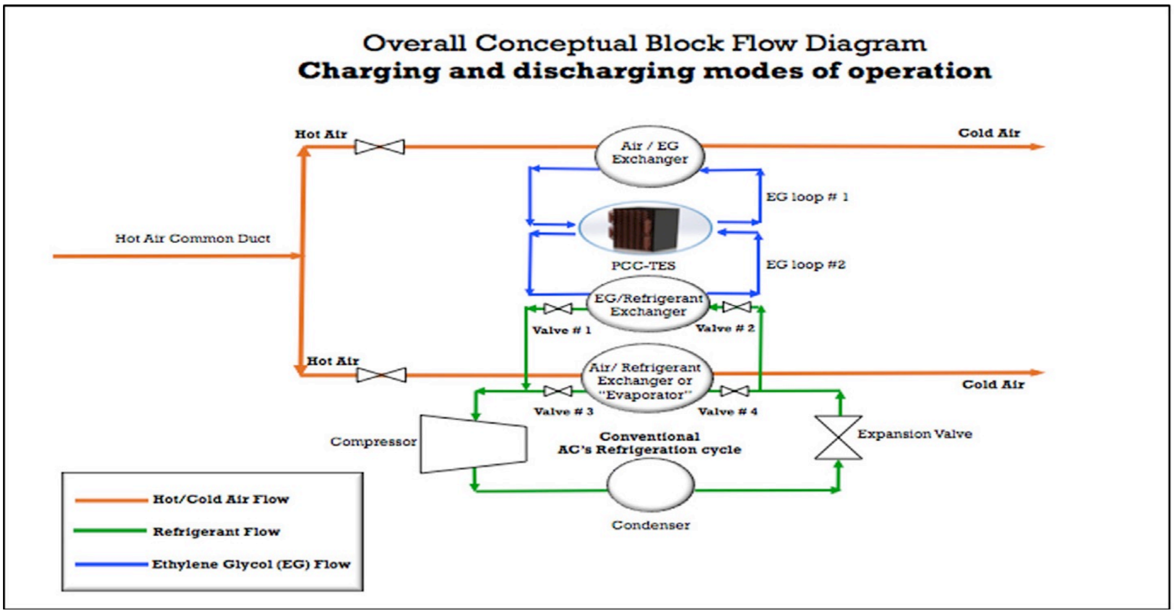

Source: ALJEHANI, NITSCHE and AL-HALLAJ, 2020

NIE *et al.*, 2020 developed work to enhance the performance of air conditioning systems with TES, as shown in **Figure 10**. They were looking for strategies to overcome the heat transfer limitations of the air and PCM, for that were considered two methods: extending heat transfer surfaces, adding fins in the PCM and airside, and adding heat transfer enhancement materials in the PCM. Fins at the surfaces are more effective than adding thermal conductive material particles in the PCM. The fins method results in enhanced of performance in the charging and discharging process. The air side fins were more effective than the PCM side fins. The results also showed that an increase in PCM thermal conductivity could enhance the heat transfer on the PCM side.

Figure 10 - Schematic diagram of experimental TES device

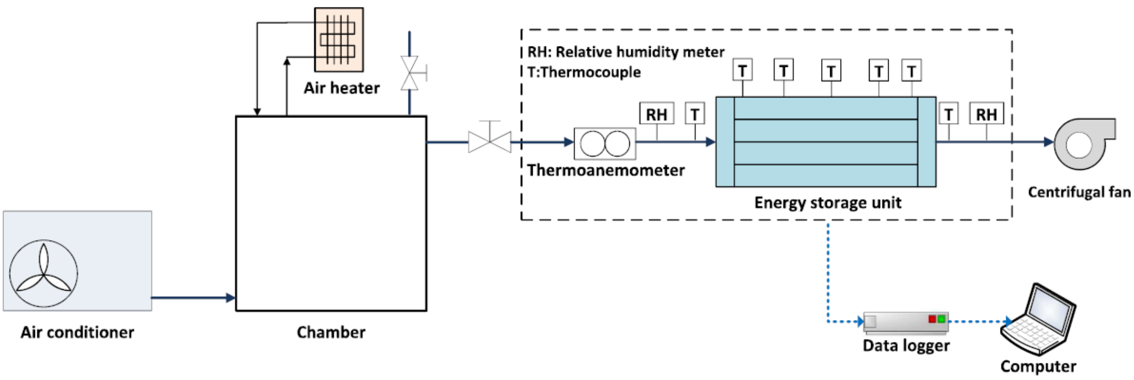

Source: NIE, DU *et al.*, 2020

The aforementioned and other studies related to the application of thermal energy storage for air conditioning systems are found in **Table 1**. It presents the papers available in the literature that integrated air conditioning and phase change materials. The information included in the table includes reference, PCM type, heat transfer fluid if the study is theoretical or experimental, and location. Furthermore, it is important to highlight that approximately 60% of the studies presented in **Table 1** used paraffin as PCM (paraffin, paraffin wax, and RT).

Table 1 – Studies on TES focused on air conditioning system

Authors	PCM	PCM's Melting Temperature (°C)	HTF	Theoretical or Experimental Study	Location
FANG, LIU and WU, 2009	Water	0	-	Experimental	-
METTAWEE, EID and AMIN, 2012	Coconut Oil	22-24	20 % ethylene glycol by volume and water	Experimental	Egypt
AL-ABIDI *et al.*, 2013	RT82	77-85	Water	Experimental	-
FASL *et al.*, 2014	Water	0	R404A	Theoretical	-
MORENO *et al.*, 2014	S10	10	Water	Experimental	Lleida (Spain)
REAL *et al.*, 2014	S10 S27	10 27	-	Experimental	Madrid, (Spain)
CHAIYAT, 2015	RT20	20–22	-	Experimental	Thailand
OSTERMAN *et al.*, 2015	RT22HC	22	Air	Experimental	Ljubljana, (Slovenia)

Authors	PCM	PCM's Melting Temperature (°C)	HTF	Theoretical or Experimental Study	Location
ZHAO and TAN, 2015	RT22	19–23	Water and air	Experimental	Laramie (USA)
QV *et al.*, 2015	RT5HC	5–6	Water	Experimental	Shanghai (China)
XIAO and ZHANG, 2015	Paraffin Paraffin composite 7 wt. % EG Paraffin composite 10 wt. % EG	60-62	Water	Experimental	-
RAHDAR, EMAMZADEH and ATAEI, 2016	RT3HC	3	-	-	Ahwaz (Iran)
ALJEHANI *et al.*, 2018	78% (C14H30) + 22% expanded graphite	4–6	Ethylene glycol	Experimental	-
LI *et al.*, 2018	HS-W1/HS- W2/Paraffin C15	4.2-5.3 / 6- 6.5 / 10	Water	Experimental	-
SAID and HASSAN, 2018	SP24E	24-25	Water	Experimental	-
AJAROSTAGHI *et al.*, 2019	Ice	0	Ethylene glycol	Theoretical	-

Authors	PCM	PCM's Melting Temperature (°C)	HTF	Theoretical or Experimental Study	Location
SAID and HASSAN, 2019	24 E/26 E/29 Eu	24–25 / 26–27 / 29–31	-	Experimental	-
ZHENG *et al.*, 2019	-	04/out	-	Experimental	Chengdu (China)
NIE *et al.*, 20200	RT18HC	17–19	Air	Experimental	-
ALJEHANI, NITSCHE and AL-HALLAJ, 2020	78% (C14H30) +22% expanded graphite	4–6	Ethylene glycol	Theoretical	-
LOEM *et al.*, 2020	RT18HC	18	-	Experimental	-
LIN *et al.*, 2021	Paraffin wax	48	Water	Experimental	-

3 METHODOLOGY

Figure 11 presents an example of a cooling system. Beyond the refrigeration system with basic components (Evaporator, Compressor, Condenser, and Expansion Device), the TES to store cold is presented. One of the main advantages of using a mathematical model is the fact that it can be used to simulate different conditions with low costs since the expenses in the simulations are generally smaller than those involved in the experimental tests, and the results are generated, for the most part, in a shorter time (DUARTE *et al.*, 2019).

Figure 11 - Air conditioning system coupled with TES

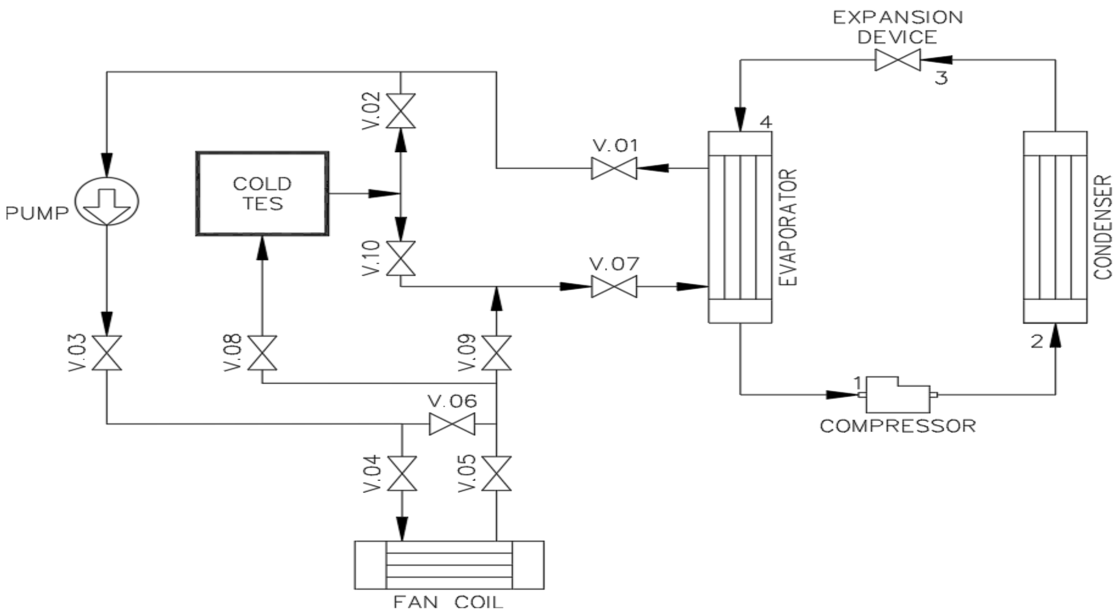

Source: Author

The cooling system is designed to match the thermal load of the environment where thermal comfort is desired. The air conditioning system, during the periods when the environmental and economic conditions are favourable for operation, the charging period, and the cold, is produced and stored in the Phase Change Material (PCM) of the TES. For charging, the secondary flow must pass through the EVAPORATOR, PUMP, and COLD TES, so valves V.01, V.03, V.06, V.08, V.10, and V.07 must be open, and all others closed. During direct operation of the air conditioner, the secondary flow must pass through the EVAPORATOR, PUMP, and FAN COIL, so valves V.01, V.03, V.04, V.05, V.09, and V.07 must be open and all others closed. During the discharge of the stored cold in the TES at peak times of electricity, the secondary flow must pass through the COLD TES, PUMP, and FAN COIL, so valves V.02, V.03, V.04, V.05, and V.08 must be open and all others closed. The mathematical model that was applied to simulate different scenarios and operating conditions and produce reliable output data is presented in **Figure 12**, **Figure 13**, and **Figure 14**.

3.1 - Compressor

The compressor is modelled with the mass flow of refrigerant at a constant rotation speed, and the consumed electrical power is given by the mathematical model of the compressor. The mass flow rate of the refrigerant ($\dot{m}_{ref}$) through the compressor is given by Eq. 1 (DUARTE *et al.*, 2019).

$$\dot{m}_{ref} = \rho_1 \,.\, N \,.\, V_{Comp} \,.\, \eta_V \qquad \text{Eq. 1}$$

Where (ρ_1) is the density of the refrigerant fluid in at the compressor inlet, (N) is the compressor rotation speed, (V_{Comp}) is the compressor displacement volume in, and (η_V) is the compressor volumetric efficiency.

The volumetric efficiency was determined according to Eq. 2, applied by for screw compressors, and the pressure ratio (r) is given by Eq. 3. In this case, "a" was assumed to be 0.95 and "b" 0.0125, as in (KOSMADAKIS *et al.*, 2020).

$$\eta_V = a - b \,.\, r \qquad \text{Eq. 2}$$

$$r = \frac{P_2}{P_1} \qquad \text{Eq. 3}$$

In the above equation, (r) is the pressure ratio, where (P_1) is the compressor inlet pressure and (P_2) is the compressor outlet pressure. The consumed electrical power of the compressor ($\dot{W}_{Comp}$) is given by Eq. 4:

$$\dot{W}_{Comp} = \dot{m}_{ref} \,.\, (i_2 - i_1) \qquad \text{Eq. 4}$$

(i_1) is the specific enthalpy of the refrigerant at the compressor inlet, and (i_2) is the specific enthalpy of the refrigerant at the condenser inlet. The compressor process was considered adiabatic, with an efficiency of 0.85.

Figure 12 - Scheme of the input and output variables of the model without storage

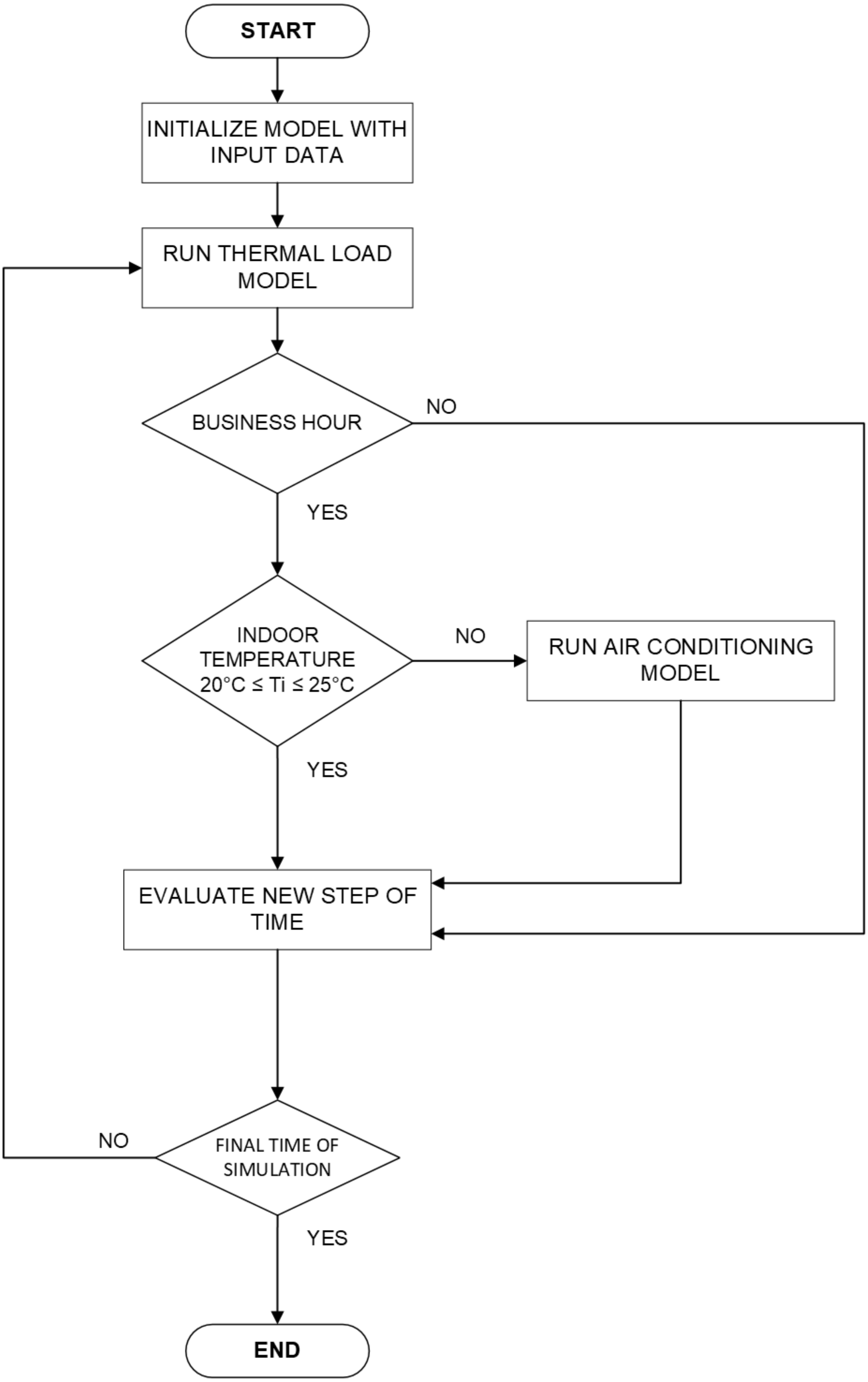

Source: Author

Figure 13 - Scheme of the input and output variables of the model with storage

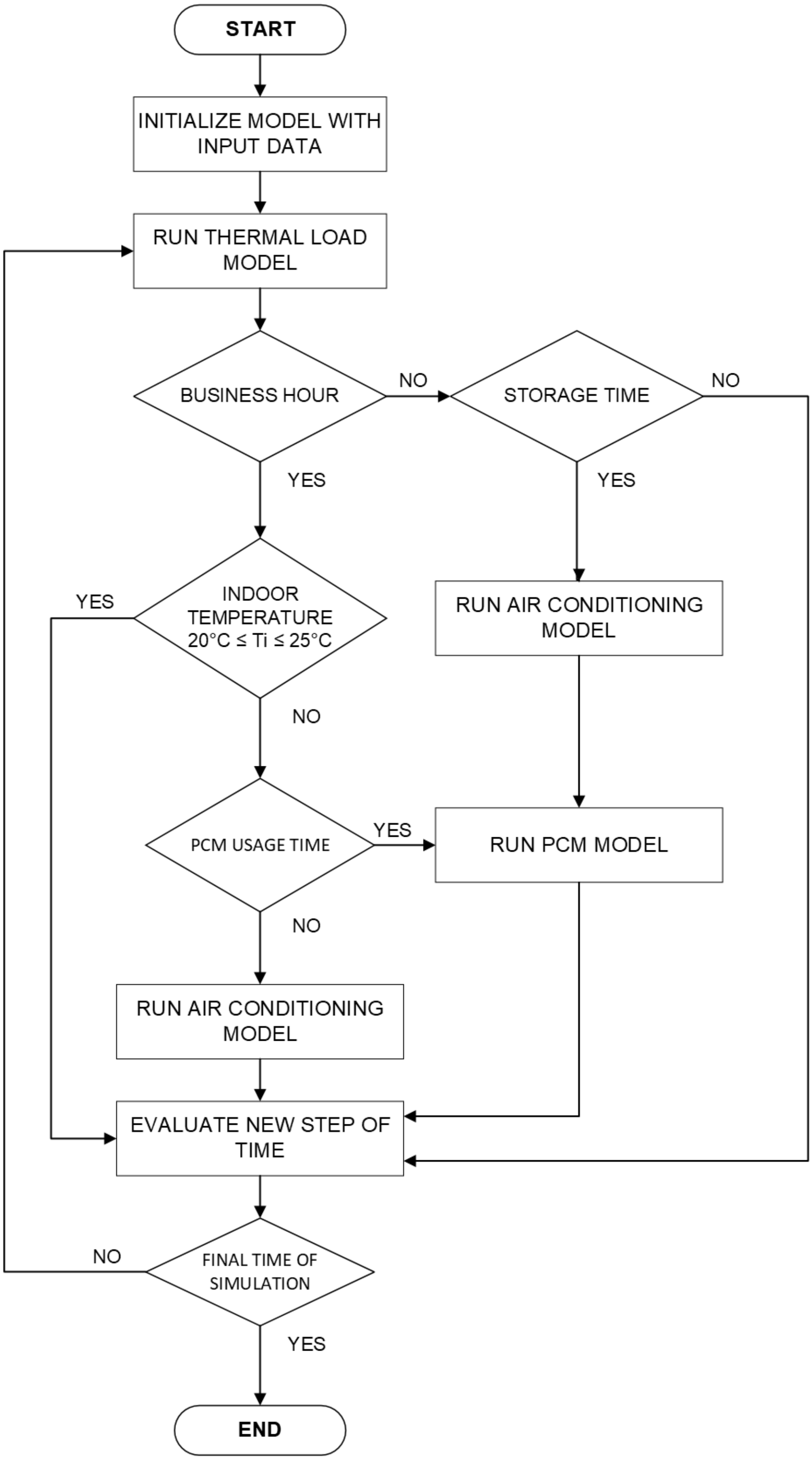

Source: Author

Figure 14 - Scheme of the input and output variables of the air conditioning model

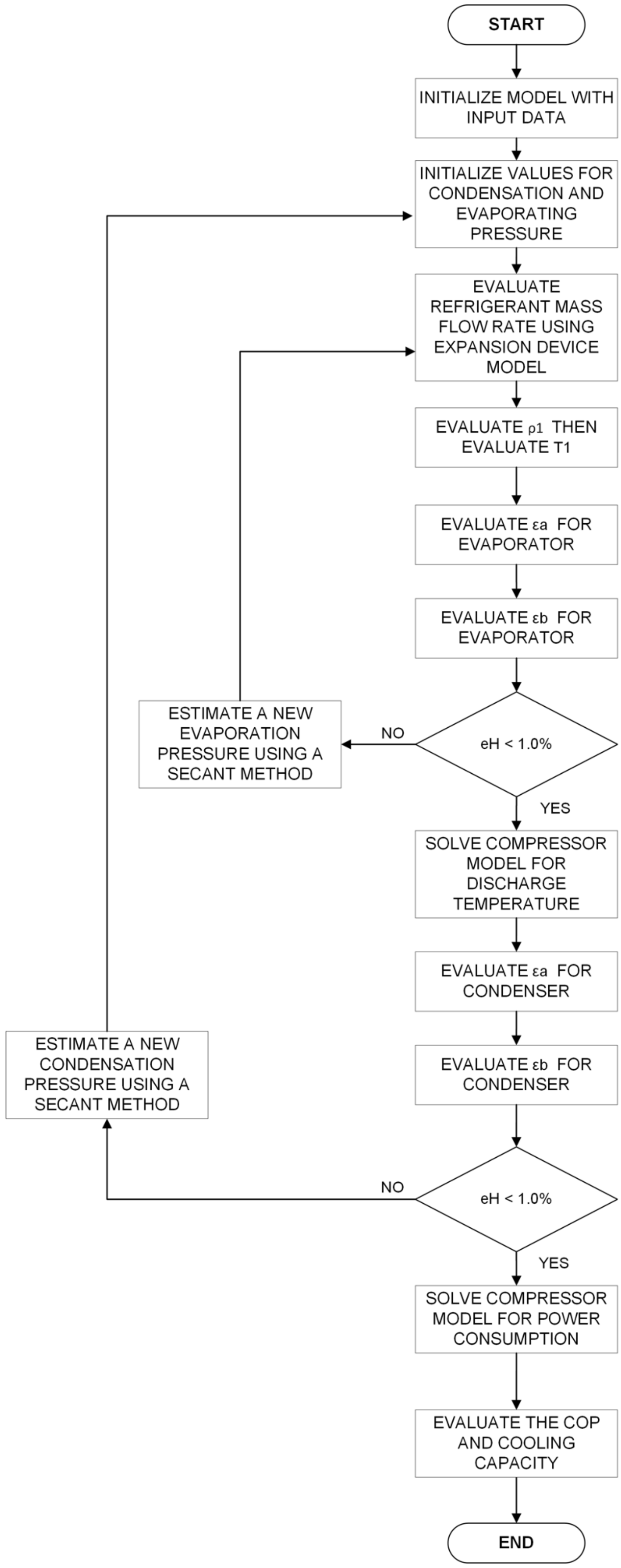

Source: Author

3.2 - Air Condenser

The condenser heat transfer rate ($\dot{Q}_{Cond}$) in the air condenser is given by Eq. 6:

$$\dot{Q}_{Cond} = \dot{m_{ref}} \,.\, (i_2 - i_3) = UA_{cond} \,.\, (T_{ref} - T_{air}) \qquad \text{Eq. 5}$$

$$\dot{Q}_{Cond} = \dot{m_{air}} \,.\, C_{p_{air}} . \Delta T_{air} \qquad \text{Eq. 6}$$

Where (i_3) is the refrigerant-specific enthalpy at the expansion device inlet given in, (T_{ref}) is the refrigerant fluid temperature at condenser in, (T_{air}) is the air temperature at condenser, ($\dot{m_{air}}$) mass flow rate of the air through condenser, ($C_{p_{air}}$) is the specific heat of air, and (ΔT_{air}) is the difference between the air temperature in the condenser and the environment.

The condenser global heat transfer coefficient (UA_{cond}) is the global heat transfer coefficient in the air condenser determined by Eq. 7.

$$UA_{cond} = \left(\frac{1}{\bar{h}_{Cond} \,.\, \pi . D_{ii\,cond} . L_{Cond}} + \frac{ln\left({D_{oi\,cond}}/{D_{ii\,cond}} \right)}{2 \,.\, \pi \,.\, k_C . L_{Cond}} + \frac{1}{\bar{h}_{air} \,.\, \pi . D_{ii\,cond} . L_{Cond}} \right)^{-1} \qquad \text{Eq. 7}$$

Where ($\bar{h}_{Cond}$) is the average convective coefficient of the refrigerant in the condenser, ($D_{ii\,cond}$) is the inner diameter of the refrigerant tube in the condenser, (L_{Cond}) is the length of the condenser tube, ($D_{oi\,cond}$) is the outer diameter of the refrigerant tube in the condenser, (k_C) is the thermal conductivity of the material of the refrigerant tube in the condenser and ($\bar{h}_{air}$) is the average air convection coefficient in the condenser.

The refrigerant average convective coefficient is determined according to the proposed by GNIELINSKI (1976) in single-phase flow and proposed by SHAH (2016) in two-phase flow. The correlation applied to find the air convective coefficient is proposed by (ZUKAUSKAS, 1972).

3.3 - Expansion device

The mathematical model of the expansion valve wants to identify the mass flow rate, which is determined by Eq. 8 (EAMES, MILAZZO and MAIDMENT, 2014):

$$\dot{m}_{ref} = A_{ED}\, C_{ED} \sqrt{2\, \rho_3 (\, P_3 - P_4)} \qquad \text{Eq. 8}$$

Where (A_{ED}) is the expansion valve cross-section area, (ρ_3) is the refrigerant density at the expansion device inlet, (P_3) is the refrigerant pressure at the expansion device inlet, and (C_{ED}) is the flow coefficient of the expansion valve, which is calculated by Eq. 9 (CHEN *et al.*, 2013):

$$C_{ED} = 0.02005 \sqrt{\rho_3} + \; 0.634\, v_4 \qquad \text{Eq. 9}$$

(v_4) is the refrigerant-specific volume at the expansion evaporator inlet.

3.4 - Evaporator

The coaxial evaporator is composed of two concentric tubes, with the refrigerant fluid flowing through the inner tube and the water flowing in the opposite direction (counterflow) through the annular region. The cooling capacity of the evaporator $(\dot{Q}_{ev})$ is obtained by the energy balance for the steady-state condition and given by Eq. 10 for the refrigerant side and Eq. 11 for the waterside.

$$\dot{Q}_{ev} = \dot{m}_{ref}\, .(i_1 - \; i_4) \qquad \text{Eq. 10}$$

$$\dot{Q}_{ev} = \dot{m}_{W;ev}.\, Cp_W.\,(T_{Wi} - T_{Wo}) \qquad \text{Eq. 11}$$

$$\dot{Q}_{ev} = UA_{ev}\, .\Delta T_W \qquad \text{Eq. 12}$$

Where (i_4) is the refrigerant-specific enthalpy at the evaporator inlet, $(\dot{m}_{W;ev})$ is the water mass flow rate at the evaporator, (Cp_W) is the water-specific heat, (T_{Wi}) is the water temperature at the evaporator inlet, (T_{Wo}) is the water temperature at the evaporator outlet, (UA_{ev}) is the evaporator cooling capacity, and (ΔT_W) is the difference between inlet and outlet water temperature.

The evaporator cooling capacity was calculated using the logarithmic mean temperature difference method, as shown in Eq. 13, according to (INCROPERA *et al.*, 2011).

$$UA_{ev} = \left(\frac{1}{\bar{h}_{ev}\, .\pi\, .D_{ii\, ev}\, .L_{ev}} + \frac{\ln(D_{oi\, ev}/D_{ii\, ev})}{2\, .\pi\, .\; k_C\, .L_{ev}} + \frac{1}{\bar{h}_{W;ev}\, .\pi\, .D_{io\, ev}\, .L_{ev}} \right)^{-1} \qquad \text{Eq. 13}$$

Where ($\bar{h}_{ev}$) is the average convective coefficient of the refrigerant in the evaporator, ($D_{ii\ ev}$) is the inner diameter of the refrigerant tube in the evaporator, (L_{ev}) is the length of the evaporator tube, ($D_{oi\ ev}$) is the outer diameter of the refrigerant tube in the evaporator, ($\bar{h}_{W;ev}$) is the average convective coefficient of the water in the evaporator, ($D_{io\ ev}$) is the inner diameter tube of the water tube.

The average convective coefficient of the refrigerant was determined by a numerical integration method with a constant enthalpy step, as presented by (ZHANG *et al.*, 2014). Furthermore, this method uses the correlations proposed by GNIELINSKI (1976) in single-phase flow and SHAH (2017) in two-phase flow.

3.5 - Convergence of Heat Exchangers

To evaluate the convergence, the effectiveness method will be applied for heat exchangers using Eq. 14 and Eq. 15.

$$\zeta_A = \frac{\dot{Q}}{\dot{Q}_{max}} \qquad \text{Eq. 14}$$

$$\zeta_B = f\left(NTU, \frac{C_{min}}{C_{max}}\right) \qquad \text{Eq. 15}$$

(ζ) is the heat leakage coefficient, ($\dot{Q}$) is the heat transfer rate, ($\dot{Q}_{max}$) is the maximum heat transfer, (NTU) is the number of transfer units, and (C) is the heat capacity at constant pressure.

3.6 - Energetic Efficiency Metric

The measured coefficient of performance of the refrigeration system (COP_R) is obtained from the following Eq. 16, and the coefficient of performance of the system, refrigeration, and cold-water system (COP_G), is given by Eq. 17, where ($\dot{W}_P$) is the cold water pump power.

$$COP_R = \frac{\dot{Q}_{ev}}{\dot{W}_{Comp}} \qquad \text{Eq. 16}$$

$$COP_G = \frac{\dot{Q}_{ev}}{\dot{W}_{Comp} + \dot{W}_P} \qquad \text{Eq. 17}$$

3.7 - Latent Thermal Energy Storage

The amount of stored energy can be determined by Eq. 18 (AKEIBER *et al.*, 2016):

$$Q = m_{PCM}\left[C_{pS}\left(T_m - T_i\right) + a_m\,\Delta H + C_{pL}\left(T_f - T_m\right)\right] \quad \text{Eq. 18}$$

Where (a_m) is the PCM fraction melted, (C_{pS}) is the specific heat capacity of PCM in solid state, (C_{pL}) is the specific heat capacity of PCM in liquid state, (ΔH) is the difference of latent heat in liquid and solid state, (m_{PCM}) of mass of PCM, (Q) is the amount of energy stored in PCM, (T_f) is the PCM final temperature, (T_i) is the PCM initial temperature, (T_m) is the PCM melting temperature and (ΔT) is the temperature difference.

3.8 - Thermal Load

The thermal load calculation has been developed based on the ABNT NBR 15220 and ABNT NBR 16401 standards and has already been presented (FERREIRA *et al.*, 2022). Eq. 19 presents the calculation of the wall area (A_{Wa}), which is determined by the room width (W), room length (Le), and room height (H) of the surrounding wall. Eq. 20 shows the calculation of the ceiling area (A_C), and Eq. 21 shows the floor area (A_F).

$$A_{Wa} = 2\,.\,(\mathrm{W} + \mathrm{Le})\,.\,\mathrm{H} \quad \text{Eq. 19}$$

$$A_C = \mathrm{W.\,Le} \quad \text{Eq. 20}$$

$$A_F = \mathrm{W.\,Le} \quad \text{Eq. 21}$$

The heat transfer rate by conduction ($\dot{Q}_{cht}$) is obtained from Eq. 22. Climatic data referring to the external air temperature ($T_{air,ext}$) were obtained from the INMET website.

$$\dot{Q}_{cht} = \left(U_{Wa}\,.\,A_{Wa} + U_F\,.\,A_F + U_C\,.\,A_C\right).\left(T_{air,ext} - T_{air,int}\right) \quad \text{Eq. 22}$$

Where (U_{Wa}) is the heat transfer rate by the walls, (U_F) is the heat transfer rate by the floor, (U_C) is the heat transfer rate by the ceiling, and ($T_{air,int}$) is the internal air temperature. The calculation of the heat generated by people ($\dot{Q}_{\mathrm{per}}$) is obtained by Eq. 23, where (Np) is the number of people and (F) the energy generated per person.

$$\dot{Q}_{\mathrm{per}} = Np\,.\,F \quad \text{Eq. 23}$$

Eq. 24 gives the heat generated by lighting ($\dot{Q}_{lig}$), where (Ilu) is the thermal load generated by lighting.

$$\dot{Q}_{lig} = Ilu.(W.Le) \quad \text{Eq. 24}$$

The thermal load imputed by the sun ($\dot{Q}_{sun}$) is obtained by Eq. 25. The hourly solar radiation in the roof (F_{s_c}) was obtained from the INMET website.

$$\dot{Q}_{sun} = \left(F_{s\_c}.A_C + F_{s\_p}.A_{Wa}\right).I\,.[time - \varphi] \quad \text{Eq. 25}$$

Where (F_{s_p}) is the wall solar factor, (I) is the hourly solar radiation, (time) is the actual time, and (φ) is the thermal delay.

Eq. 26 presents the calculation of the thermal load due to the air renewal rate ($\dot{Q}_{arr}$). The air-specific mass (ρ_{air}) and the air enthalpy of the external ($i_{ar,ext}$) and internal ($i_{ar,int}$) environment are obtained from CoolProp.

$$\dot{Q}_{arr} = \rho_{air}\,.\left(F_p\,.Np + F_a\,.A_{Wa}\right).\left(i_{air,ext} - i_{air,int}\right) \quad \text{Eq. 26}$$

Where (F_p) is the air renewal factor per person and (F_a) is the air renewal factor per area. Finally, the hourly thermal load rate ($\dot{Q}_e$) is obtained by Eq. 27

$$\dot{Q}_e = \dot{Q}_{\text{per}} + \dot{Q}_{lig} + \dot{Q}_{sun} + \dot{Q}_{arr} + \dot{Q}_{cht} + \dot{Q}_{\text{ele}} \quad \text{Eq. 27}$$

Where ($\dot{Q}_{\text{ele}}$) is the heat transfer rate by equipment. The general input data for the calculation of the thermal load are shown in **Table 3**.

3.9 - Work to be developed

The model considers a time step of 2 minutes between the simulations carried out, for each step of the simulation the calculation of the thermal load of the environment was carried out, with the information of the thermal load the temperature of the environment is calculated, if this temperature is higher than the limit defined as comfort temperature, a simulation of the air conditioning system is carried out to reduce the temperature and keep it within the defined parameters.

Given the aforementioned information, the work that follows from here will be focused on carrying out the implementation of the mathematical model of the equations presented to determine the thermal load of an office environment with the dimensions according to **Table 2**. The environment will be considered for simulation in Teresina (NE) in Brazil.

The simulation of the mathematical model of the refrigeration system was carried out in the Python programming language using thermodynamic data from the CoolProp library, for which the data shown in **Table 3**, **Table 4,** and **Table 5** were used. The simulation of the refrigeration system is carried out taking into account the appropriate moment for the storage of the generated cold by the TES (TES charge) according to **Figure 13,** the simulation of the refrigeration system with direct consumption of the cold by the environment according to **Figure 12,** the moment when the environment is acclimatized by the cold stored in the TES (TES discharge).

Table 2 – Surrounding input data

Input data	Value
Room width (W)	8,0 m
Room Length (L)	6,0 m
Room height (H)	2,8 m
Number of computers	19
Number of additional monitors for computers	19
Number of large printers	2
Number of coffee machines	1
Number of people (N)	22

Source: Author

For the simulation of the air conditioning system, the city of Teresina, located in the state of Piauí (PI) in the northeast of Brazil, was chosen. The climate data for Teresina was obtained from the website of the Brazilian National Institute of Meteorology (INMET) for the year 2019. It was determined that the environment should be air-conditioned during business hours from 08:00 to 18:00, with the room temperature maintained between 20.0°C and 25.0°C during this period. The air conditioning system coupled to the TES charged during the night shift and then discharged the TES during the afternoon shift.

An evaluation of the meteorological data available for the city for the year 2019 was carried out on select days for analysis. This analysis focused on global radiation and air temperature. After evaluating these main meteorological data, the day of 23.01.2019 was selected because it has the highest radiation. The day of 20.12.2019 was selected because it has the highest temperature. In addition, the day of 17.05.2019 was chosen because it has the lowest maximum temperature recorded.

Table 3 – General input data

Description	Input Data	Reference
Heat transfer rate by the walls (U_{Wa})	2.58 W/(m²K)	ABNT, 2005. NBR15220-3
Heat transfer rate by the floor (U_F)	1.59 W/(m²K)	ABNT, 2005. NBR15220-3
Heat transfer rate by the ceiling (U_C)	1.92 W/(m²K)	ABNT, 2005. NBR15220-3
Absorbency for wall with white paint (α_W)	0,2	ABNT, 2005. NBR15220-2
Absorbency for galvanized steel sheet roof (α_c)	0,25	ABNT, 2005. NBR15220-2
Thermal capacitance of the internal environment (C_{in})	2,250.0 kJ/K	
Thermal delay (φ)	3 h	ABNT, 2005. NBR15220-3
Roof solar factor (F_{S_C})	0,065	ABNT, 2005. NBR15220-3
Wall solar factor (F_{S_P})	0,035	ABNT, 2005. NBR15220-3
Air renewal factor per person (F_p)	3,8 (m³/s)/person	ABNT, 2008. NBR16401-1
Air renewal factor per area (F_a)	0,5 (m³/s)/m²	ABNT, 2008. NBR16401-1
Thermal load generated by lighting per square meter of building (Ilu)	16 W/m²	ABNT, 2008. NBR16401-1
Thermal load generated in a computer	55 W	ABNT, 2008. NBR16401-1
Thermal load generated in a small printer	130 W	ABNT, 2008. NBR16401-1
Thermal load generated in a large printer	550 W	ABNT, 2008. NBR16401-1
Additional monitor	55 W	ABNT, 2008. NBR16401-
Coffee machine	1500 W	ABNT, 2008. NBR16401-
Energy generated per person (F)	130 W	ABNT, 2008. NBR16401-1

Source: Author

Table 4 – TES input data

Input data	Value
PCM	Paraffin wax
Specific heat capacity of PCM in solid state (C_{ps})	2.01 kJ/(kg . K)
Specific heat capacity of PCM in liquid state (C_{pL})	4.18 kJ/(kg . K)
Mass of PCM (m_{PCM})	250 kg
Difference of latent heat in liquid and solid state (ΔH)	333.6 kJ/kg)
PCM melting temperature (T_m)	278.15 K
PCM final temperature (T_f)	277.15 K
Secondary fluid	Ethylene glycol 6.5%
Pipe diameter	2" – SCH80
Length (between the evaporator and fan coil)	30 m
Length (between evaporator and TES)	10 m
Length (between TES and fan coil)	35 m
Water pipe roughness	0.0023 mm
Ethylene Glycol 6.5% inlet temperature in the TES for charging	271.15 K
Ethylene Glycol 6.5% outlet temperature in the TES for charging	276.15 K
Ethylene Glycol 6.5% inlet temperature in the TES for discharging	280.15 K
Ethylene Glycol 6.5% outlet temperature in the TES for charging	285.15 K

Source: Author

Table 5 – Refrigeration cycle input data

Input data	Value
Fluid	R134a
Subcooling	5.0 K
Superheating	7.0 K
Compressor manufacturer	EMBRACO
Compressor model	SE6089GS-O
Compressor stroke	197.1 x 10^{-6} m³/rev
Compressor speed	2900 rev/min
Compressor isentropic efficiency (η_{is})	0.85
Water pump efficiency (η_p)	0.85
The outer diameter of the refrigerant tube in the condenser ($D_{ei\ cond}$)	9.52 x 10^{-3} m
The inner diameter of the refrigerant tube in the condenser ($D_{ii\ cond}$)	7.67 x 10^{-3} m
Length of the condenser tube (L_{Cond})	50.0 m
Air condenser face area	3.05 m²,
Air condenser maximum speed correction factor	2.0
Air condenser airflow	1.500 m³/h
Expansion device cross-section area (A_v)	2.0 x 10^{-6} m²
Water flow rate at the evaporator	0.012 L/s
Water inlet temperature in the evaporator (T_{Wi})	285.15 K
Water outlet temperature in the evaporator (T_{Wo})	280.15 K
Outer diameter of the refrigerant tube in the evaporator ($D_{ei\ ev}$)	19.05 x 10^{-3} m
Inner diameter of the refrigerant tube in the evaporator ($D_{ii\ ev}$)	17.47 x 10^{-3} m
Outer diameter of the water tube in the evaporator ($D_{oe\ ev}$)	22.22 x 10^{-3} m

Input data	Value
Inner diameter of the water tube in the evaporator ($D_{ie\ ev}$)	20.64 x 10^{-3} m
Length of the evaporator tube (L_{ev})	25.0 m
Thermal conductivity of the material (copper) (k_C)	396 W/(m.K)
Refrigerant pipe roughness	0.0015 x 10^{-3} mm

Source: Author

Figure 15 – Total daily global solar radiation

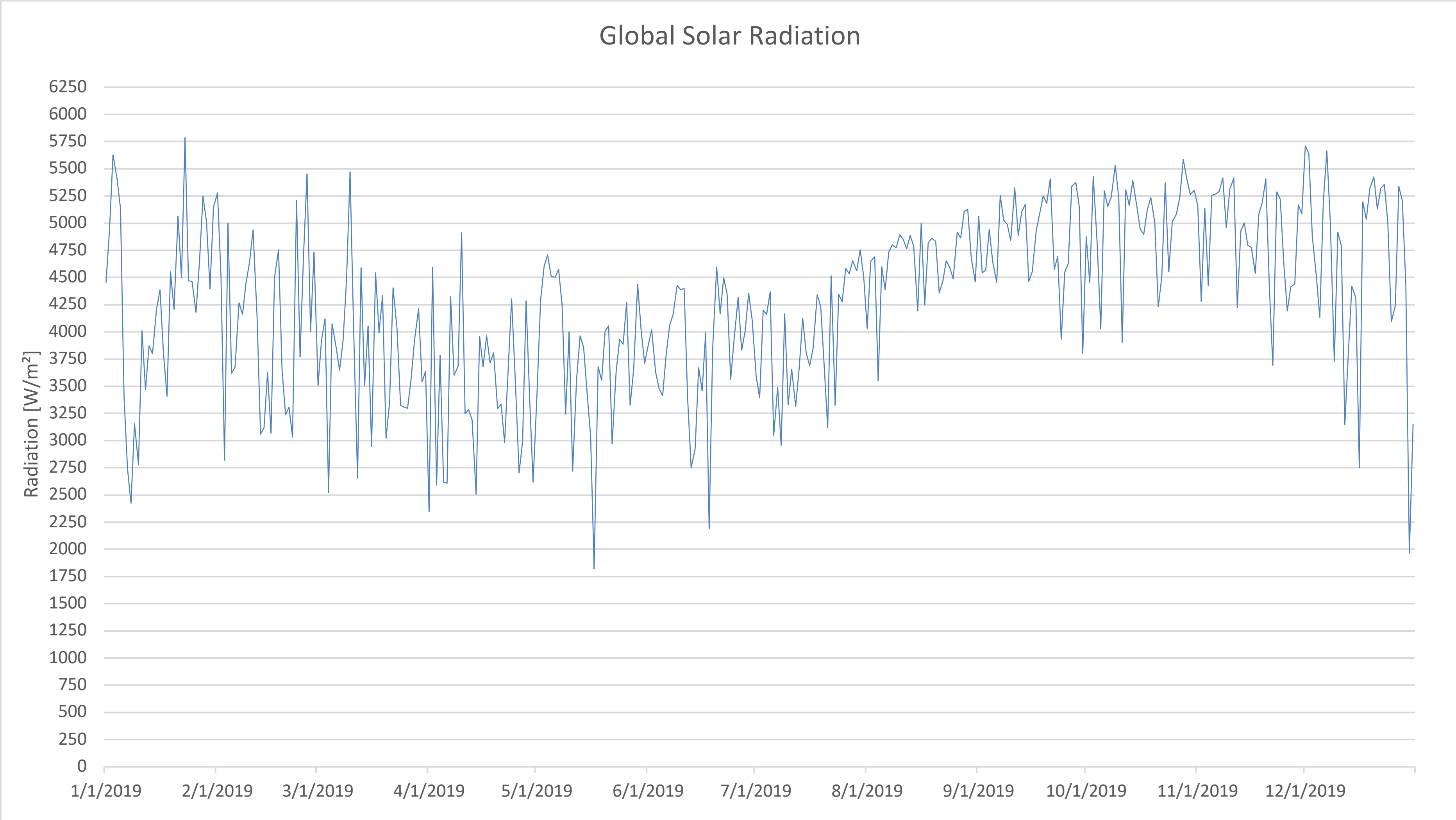

Source: Author

Figure 16 - Air Temperature - Dry Bulb - Daily Maximum

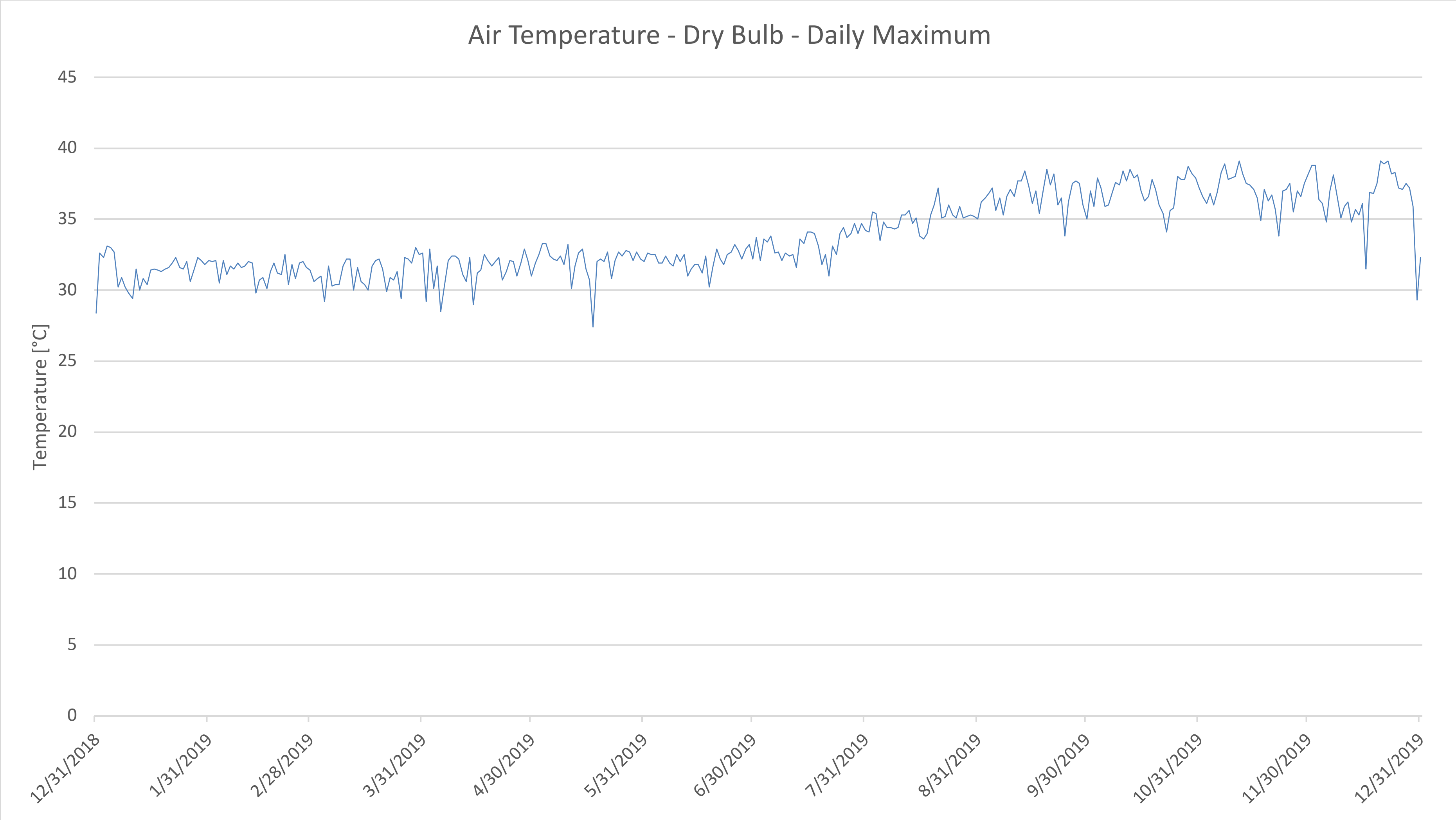

Source: Author

4 RESULTS

The simulated results are described in this section. The thermal performance of the air conditioning system was numerically simulated during a selected day in the climatic conditions of Teresina - PI.

The day analysed was the 23.01.2019, which has the highest radiation rate. The solar radiation of this day is shown in **Figure 17**, and the effect of radiation can be noted in the internal temperature. **Figure 18** shows the external and internal temperatures (with and without TES) of the simulated environment. Approximately three hours after the radiation rate started, the heat gain of the environment increased. At the beginning of the business hour, it decreases because the air conditioning system starts to work. In the operation of the air conditioning system without the use of the TES, the temperature varies between the set limits, from 20°C to 25°C, throughout the entire operating cycle of the system since the air conditioning system is coupled to the TES, the temperature at the beginning of the TES discharge period is maintained since the simulation has determined that all the thermal load generated from 13:00 onwards should be deducted from the energy stored in the TES until all of it is consumed.

Figure 17 - Radiation – 23.01.2019

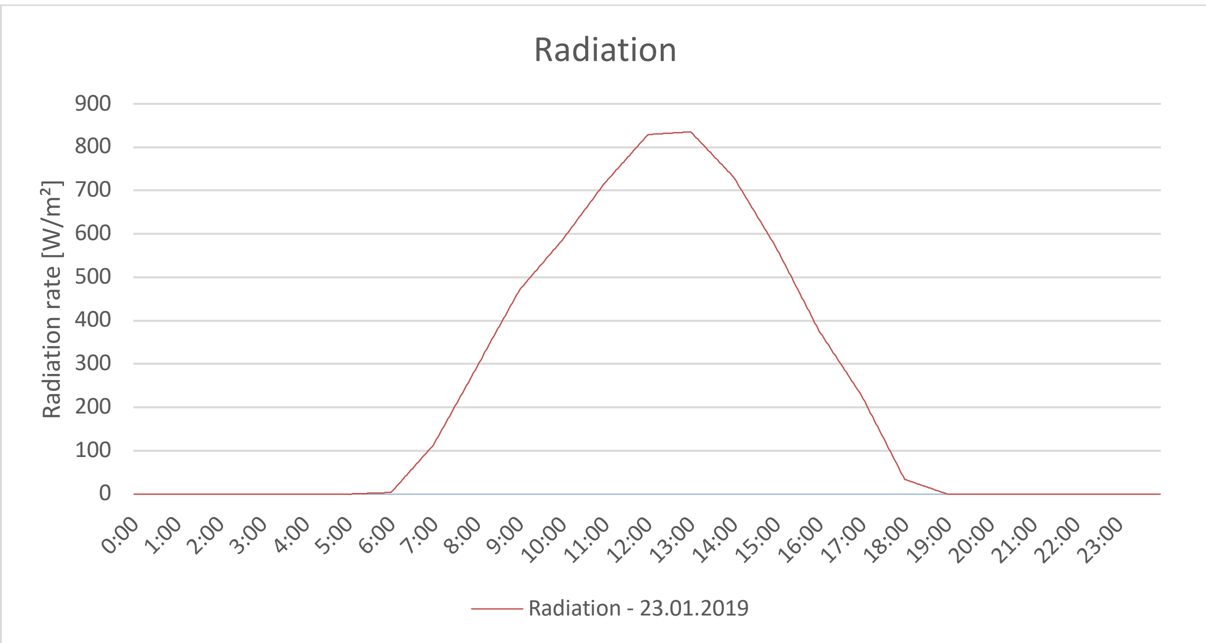

Source: Author

Figure 18 - Internal and external temperature – 23.01.2019

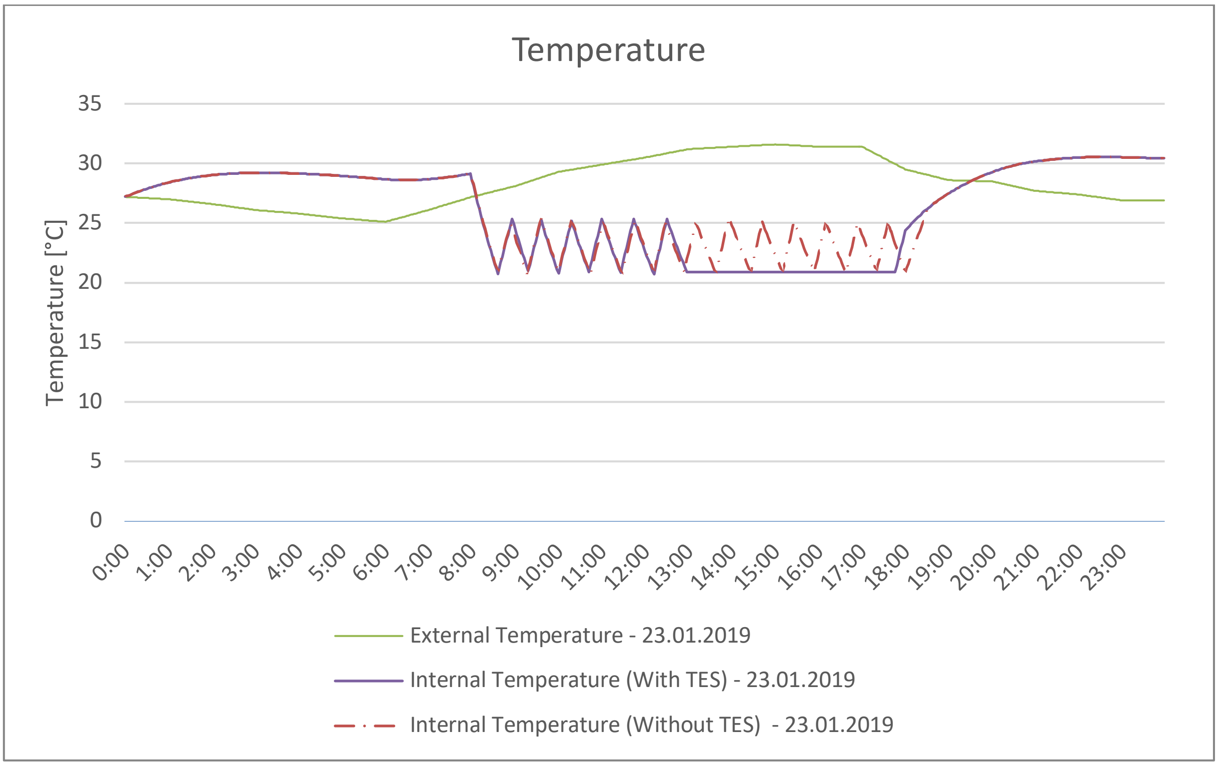

Source: Author

The three following figures show the behaviour of the PCM during charging, storage, and discharging. During charging, from 01:00 to 04:00, an increase in stored energy can be seen in **Figure 21**. At the start of the charging process, the material temperature drops, **Figure 20**, as does the start of the solidification process. Although the solidification process starts quickly during loading, only 2.6% of the mass of 250.0 kg of PCM solidifies, as shown in **Figure 19**. From 04:00 to 13:00, we have the PCM energy storage phase, during which the accumulated energy is maintained, as is the temperature and solidification. After 13:00, the PCM discharge process begins. At the beginning of the process, the temperature remains constant, while the stored heat and the solid fraction are reduced until all the stored heat is slaughtered by the thermal load of the environment.

Figure 19 - PCM solid fraction – 23.01.2019

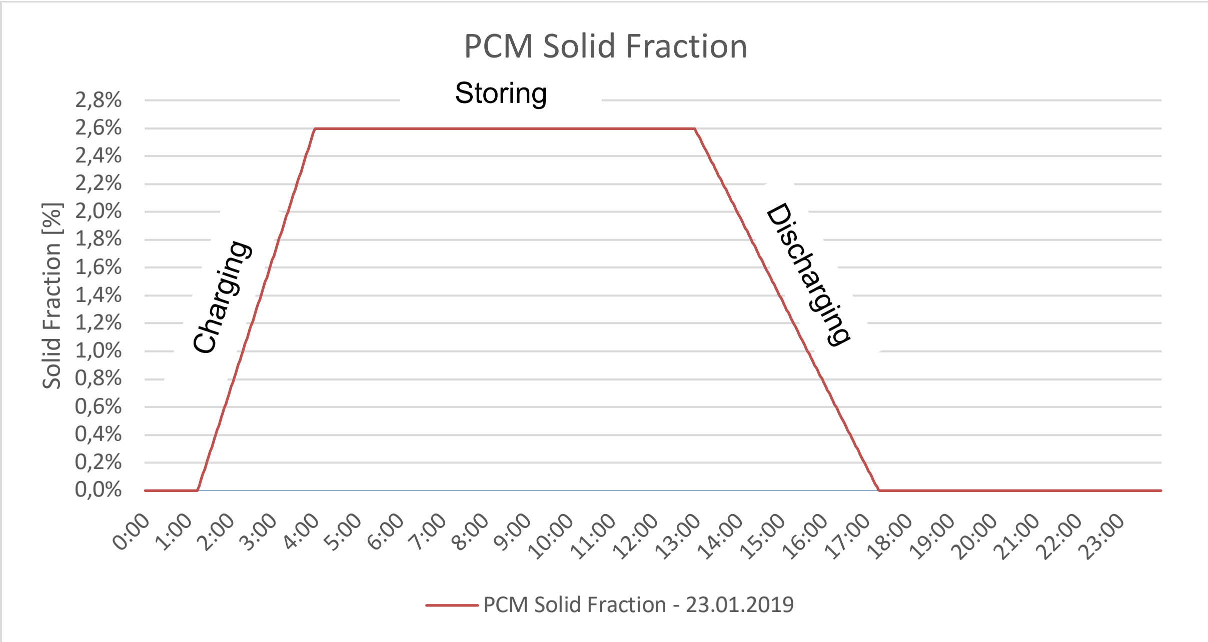

Source: Author

Figure 20 - PCM temperature – 23.01.2019

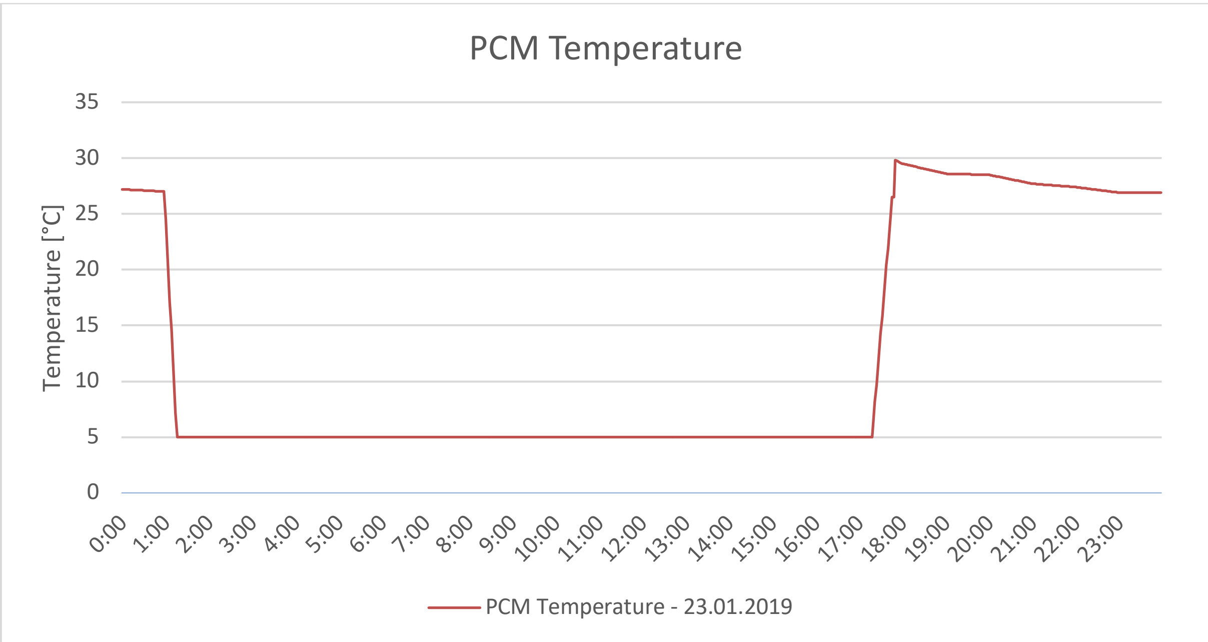

Source: Author

Figure 21 - PCM stored heat – 23.01.2019

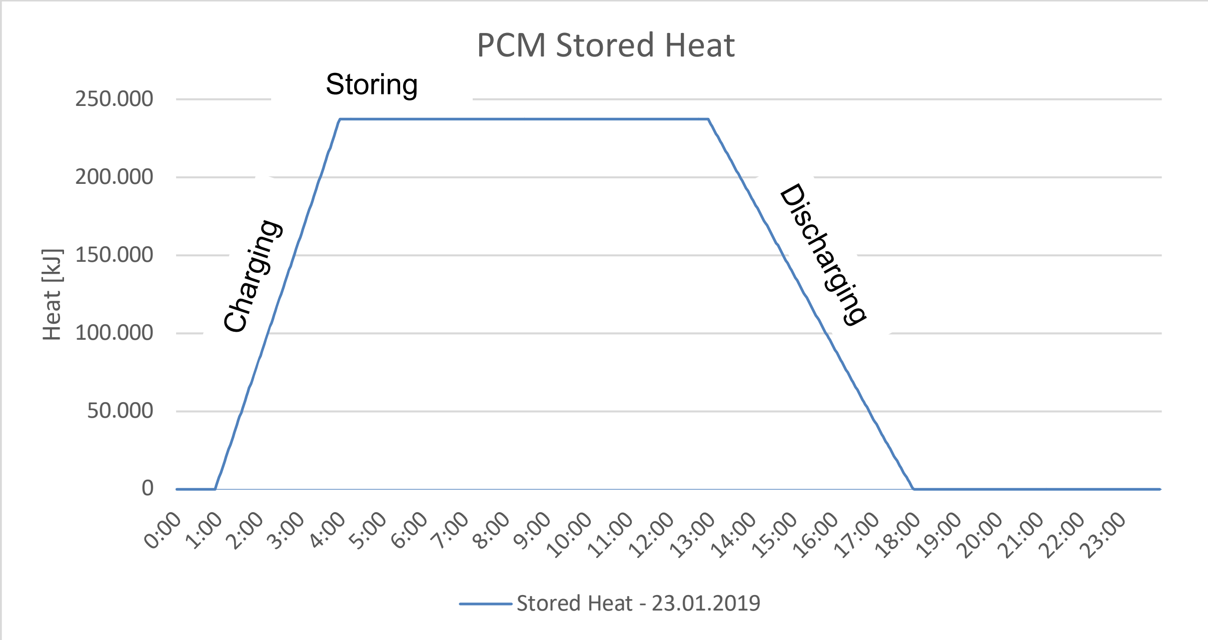

Source: Author

The efficiency of the operation of the air conditioning system on 23.01.2019 can be seen in **Figure 22** and **Figure 23**, where the COP_R values are shown. The air conditioning system coupled with the TES has the same values COP_R values as the system without the TES during the period the business hour when the TES is not discharging; on the other hand, the COP_R average is 77.1% lower during the discharging period, 13:00 to 18:00, when compared to the charging period of the TES 01:00 to 04:00. The higher COP_R values observed during the charging period of the TES are because cooling is easier during the night when outside temperatures are usually lower. During business hours, the COP_Rs are the same as long as the air conditioner is the same.

The COP_G was considered in this simulation; during the charging period, the highest value of this was 1.95, and the average was 1.93, which is 69.5% higher than the average for the system without TES during the discharging period, which had the highest value of 1.83.

Figure 22 - System without TES - COP – 23.01.2019

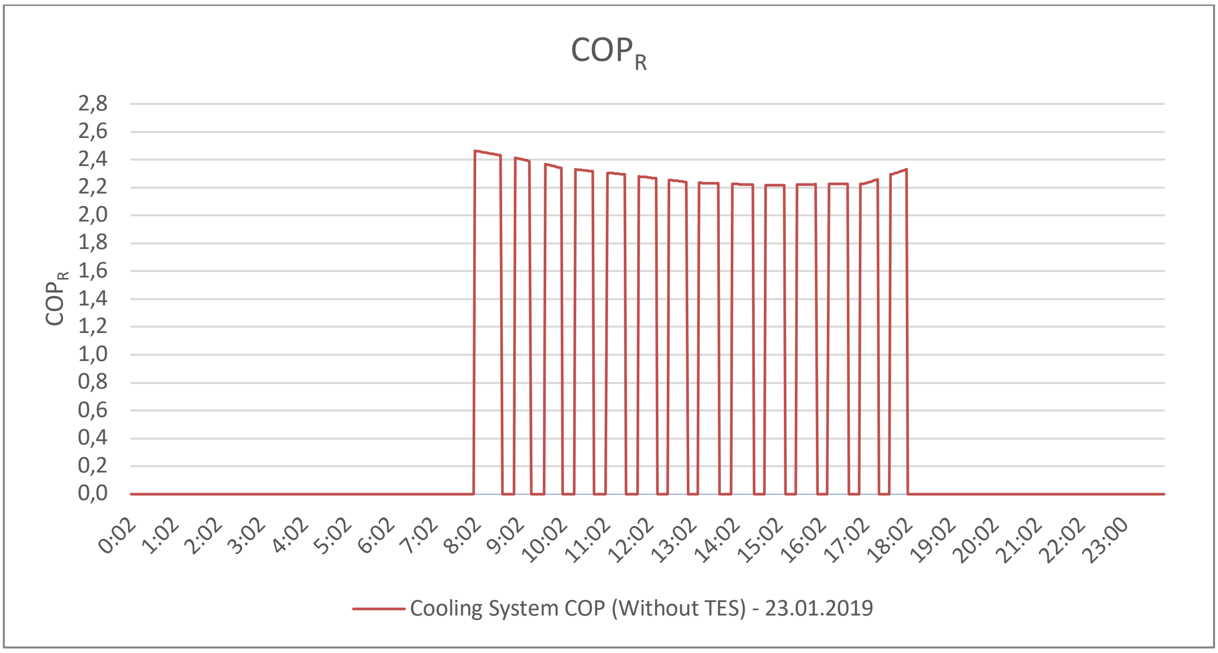

Source: Author

Figure 23 - System with TES - COP – 23.01.2019

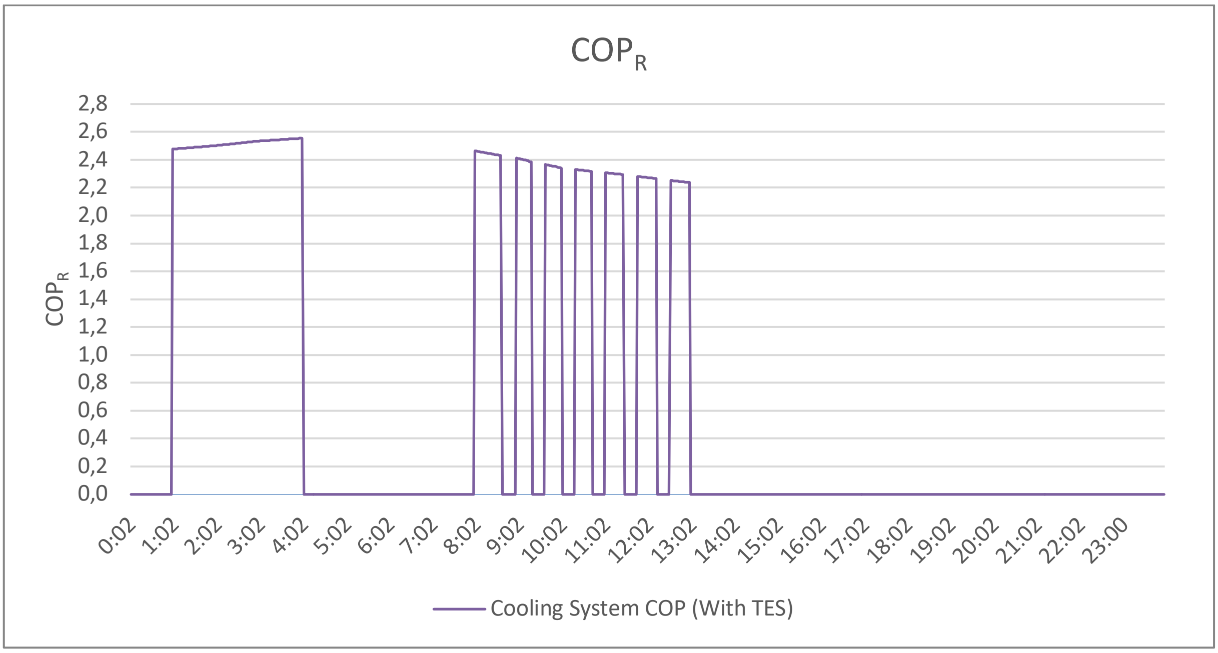

Source: Author

Although the air conditioning system has done the work of producing cooling during the loading period and is still running for part of the business hours, from 08:00 to 13:00, the pump has been working during the entire TES unloading period, the air conditioning system coupled with TES has a total energy consumption at the end of the day that is lower than the system that is not coupled, as shown in **Figure 24**. We can see that the energy consumed by the pump in the air-conditioning system with TES is higher than in the system without TES because the pump remains in operation during the TES discharge period, so we have that the pump, in addition to working during the system charging period, also remains in operation during the working hours. For 23/01/2019, an air conditioner with TES saves 3.4% in electricity consumption.

Figure 24 – Power Consumption – 23.01.2019

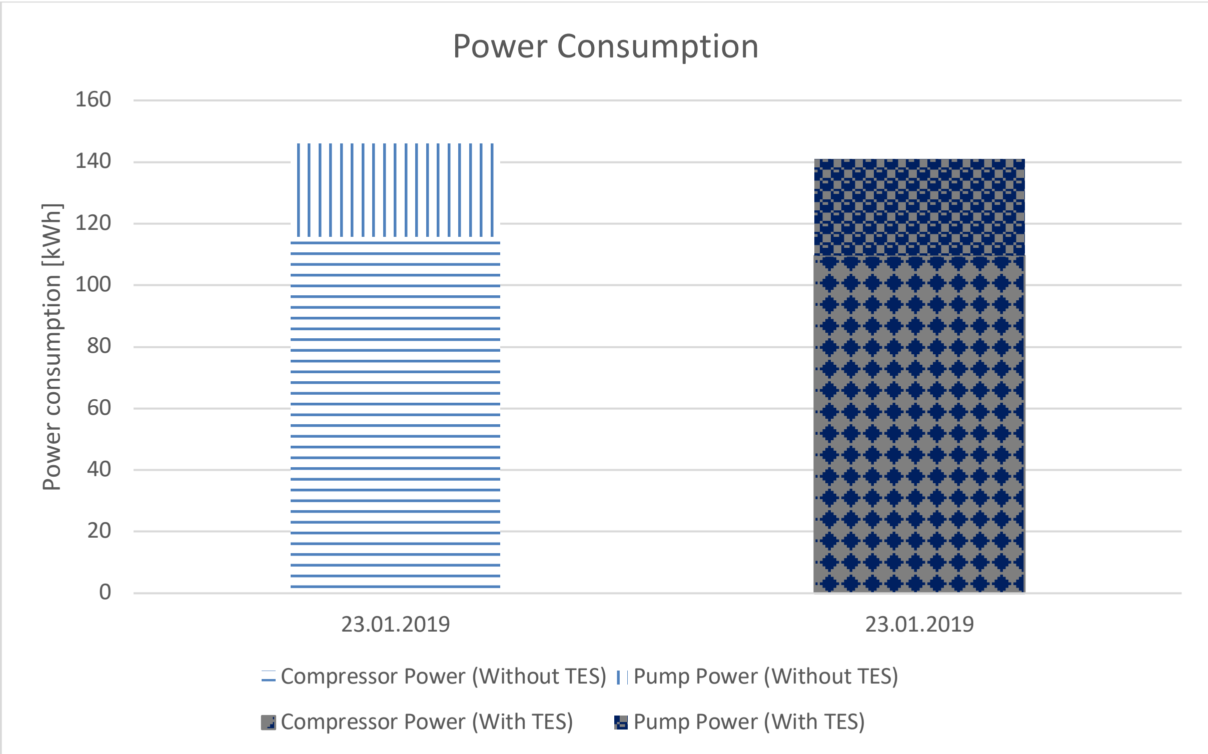

Source: Author

The highest temperature occurred three times during the year, one of which was the day 20.12.2019. **Figure 25** shows the external and internal temperatures of the simulated environment. For this day, the discharge period of the TES starts when the internal temperature is close to the temperature of the upper limit of the setpoint. As shown in **Figure 26**, the stored heat was not enough to supply the total thermal load during the discharge period, so the air conditioning had to start working again, and the internal temperature started to decrease again.

Figure 25 - Internal and external temperature – 20.12.2019

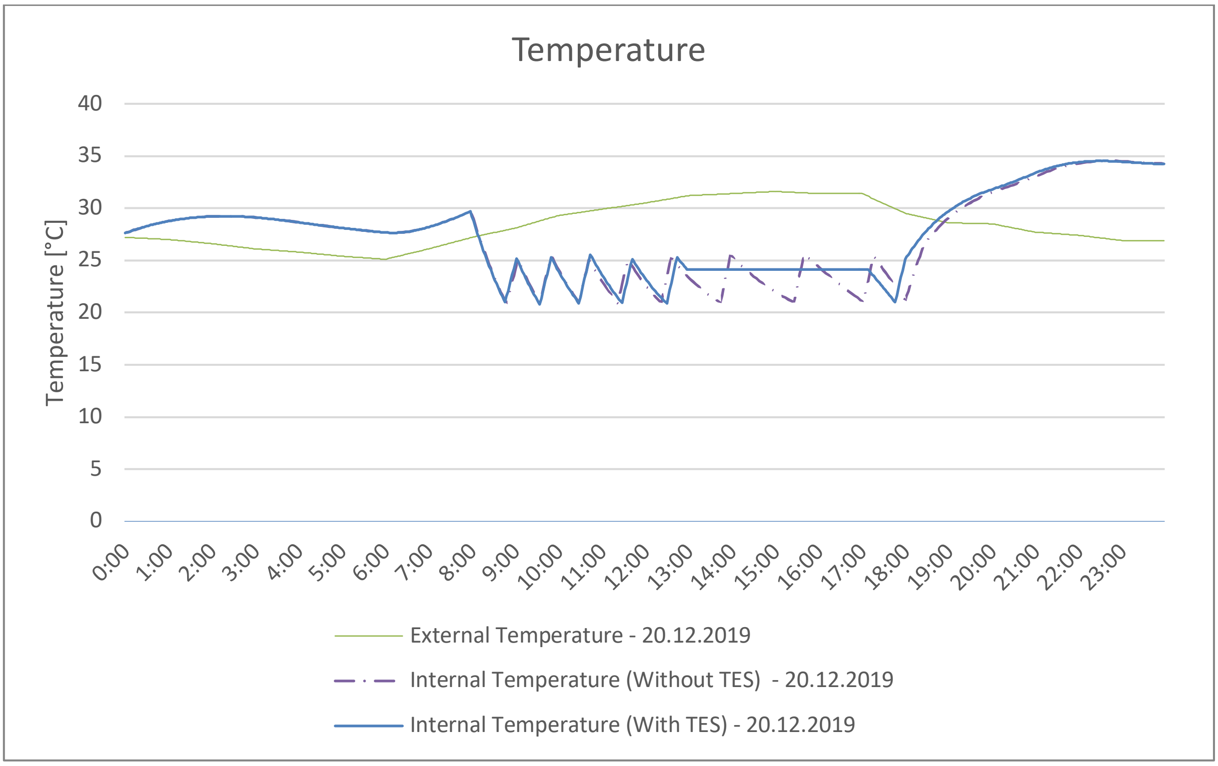

Source: Author

Figure 26 - PCM stored heat – 20.12.2019

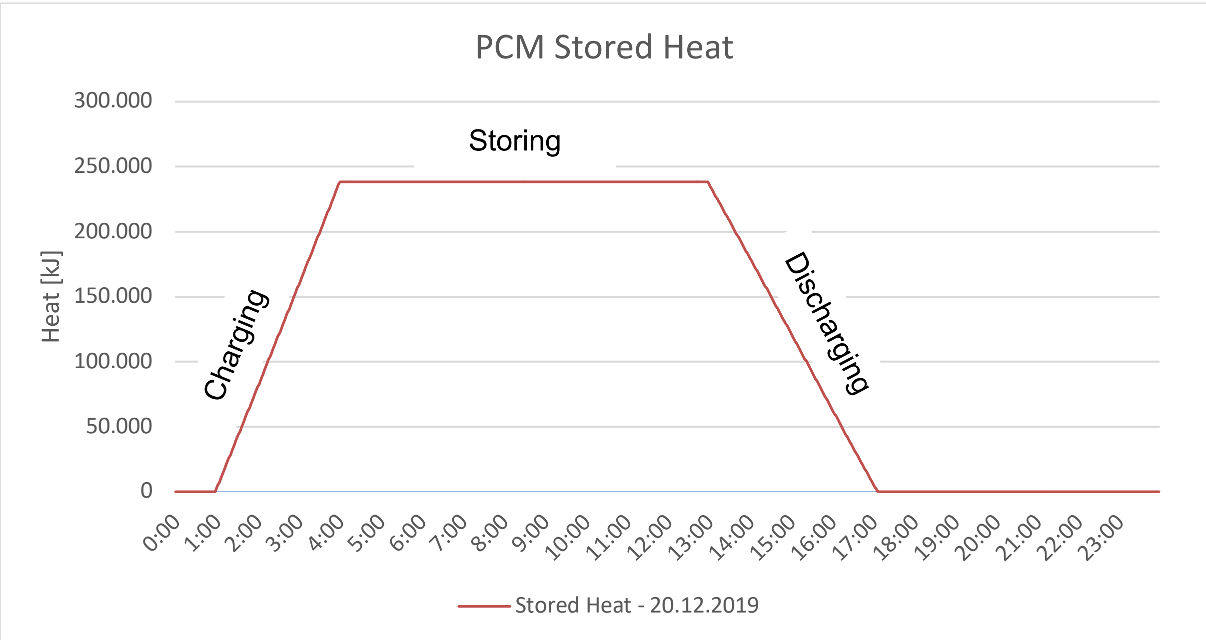

Source: Author

As aforementioned, the stored heat was not sufficient for the whole discharge period, from 13:00 to 18:00. **Figure 27** shows the PCM solid fraction; it can be seen that all the PCM of the TES was melted before the end of the discharge period and at the **Figure 28** the temperature of the PCM starts to increase until it reaches the external temperature, once the TES is discharged the flow no longer flows through the TES.

Figure 27 - PCM solid fraction – 20.12.2019

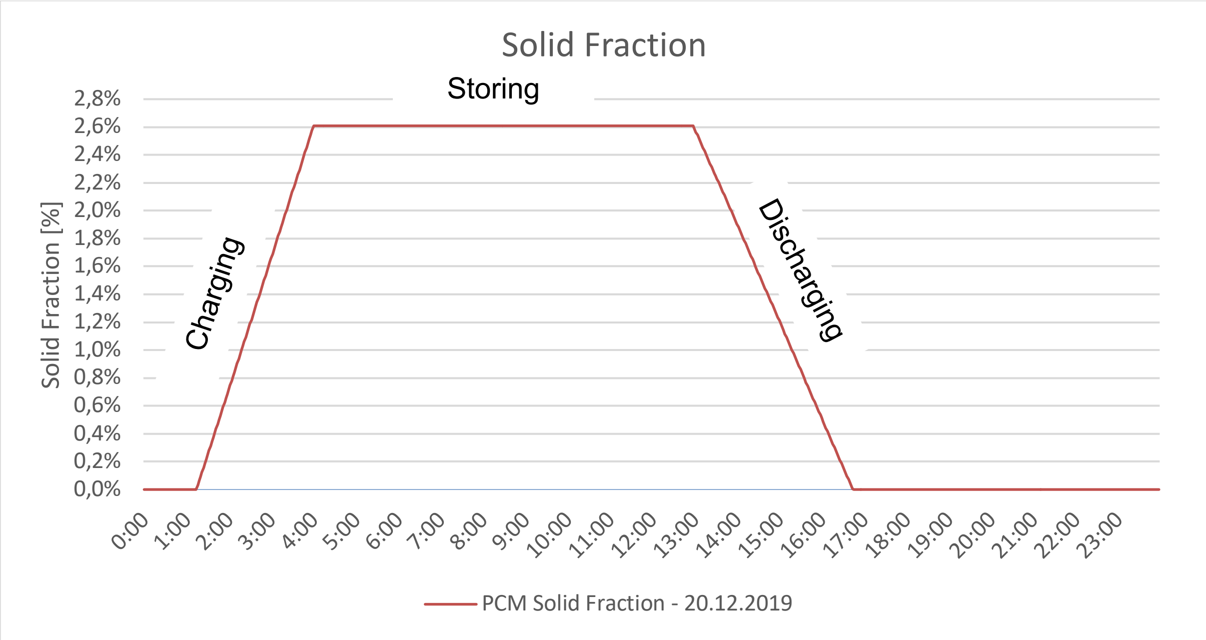

Source: Author

Figure 28 - PCM temperature – 20.12.2019

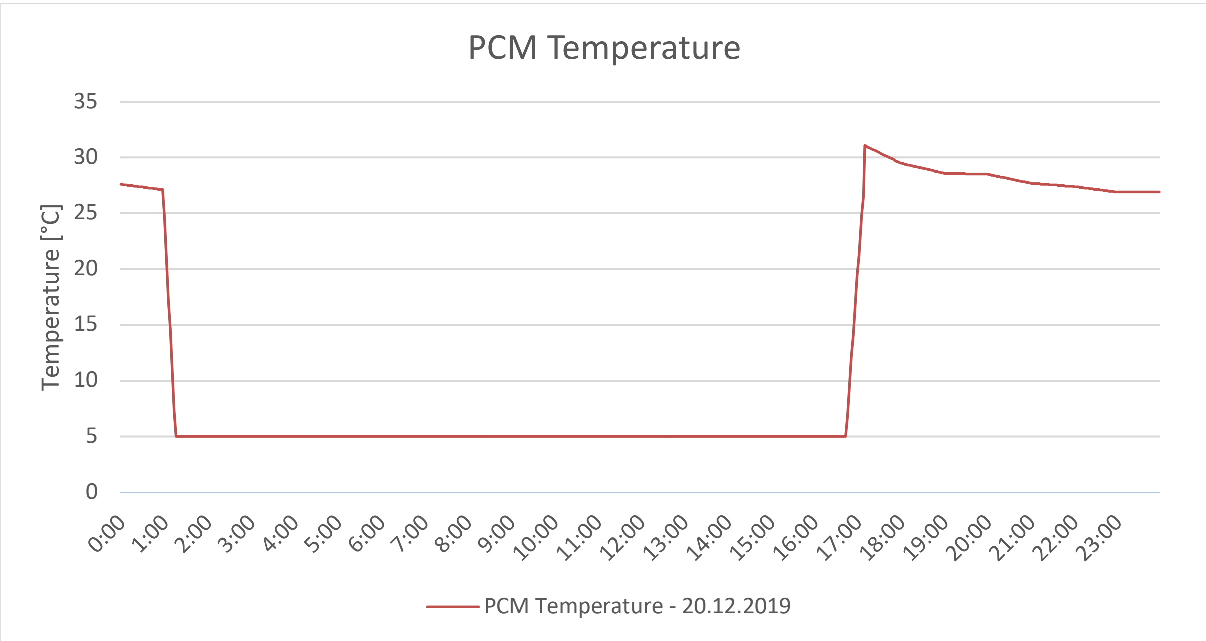

Source: Author

The efficiency of the operation of the air conditioning system operation in 20.12.2019 can be seen in **Figure 29** and **Figure 30**, where the COP_R values are shown. The air conditioning system coupled with the TES has COP_R average of 54.6% higher during the charging period, from 01:00 to 04:00 than during the discharging, from 13:00 to 18:00, for the system without TES. The higher COP_R value observed during the charging period of the TES is 2.63, and the average during this period is 2.55. During business hours, the COP_R of the air conditioning system with TES reappears when the system starts working at the end of the afternoon.

The COP_G was considered in this simulation; during the charging period, the highest value of this was 1.98, and the average was 1.94, which is 45.8% higher than the average for the system without TES during the discharging period, which had the highest value of 1.83.

Figure 29 – System without TES - COP – 20.12.2019

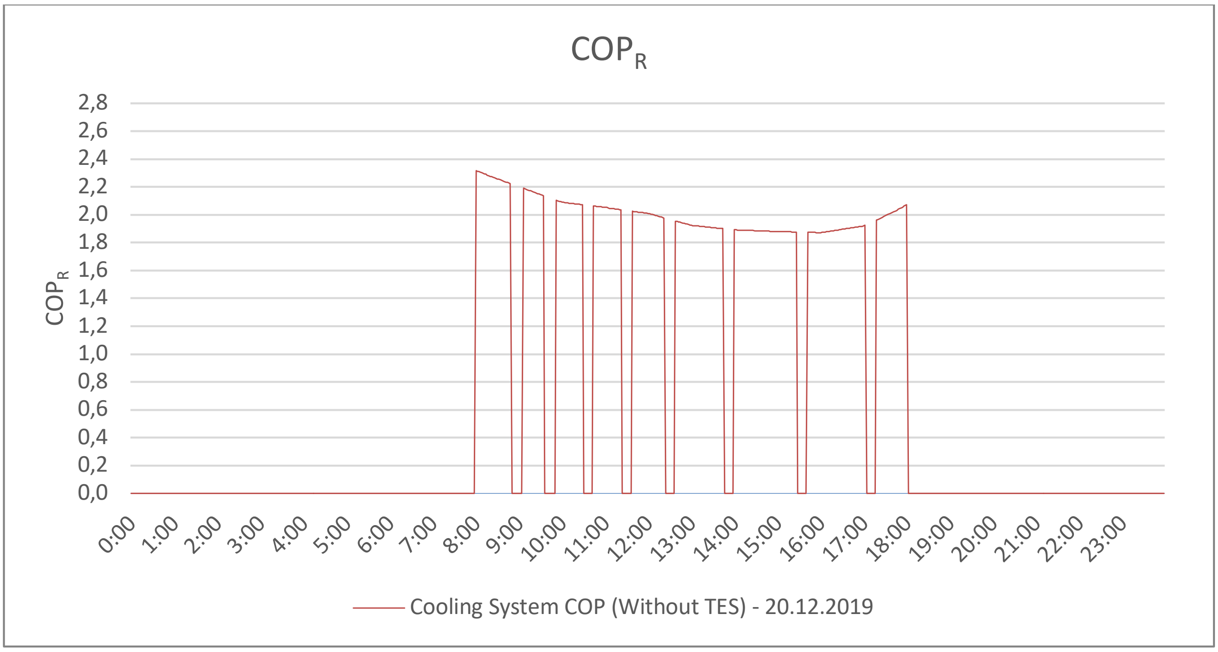

Source: Author

Figure 30 – System with TES - COP – 20.12.2019

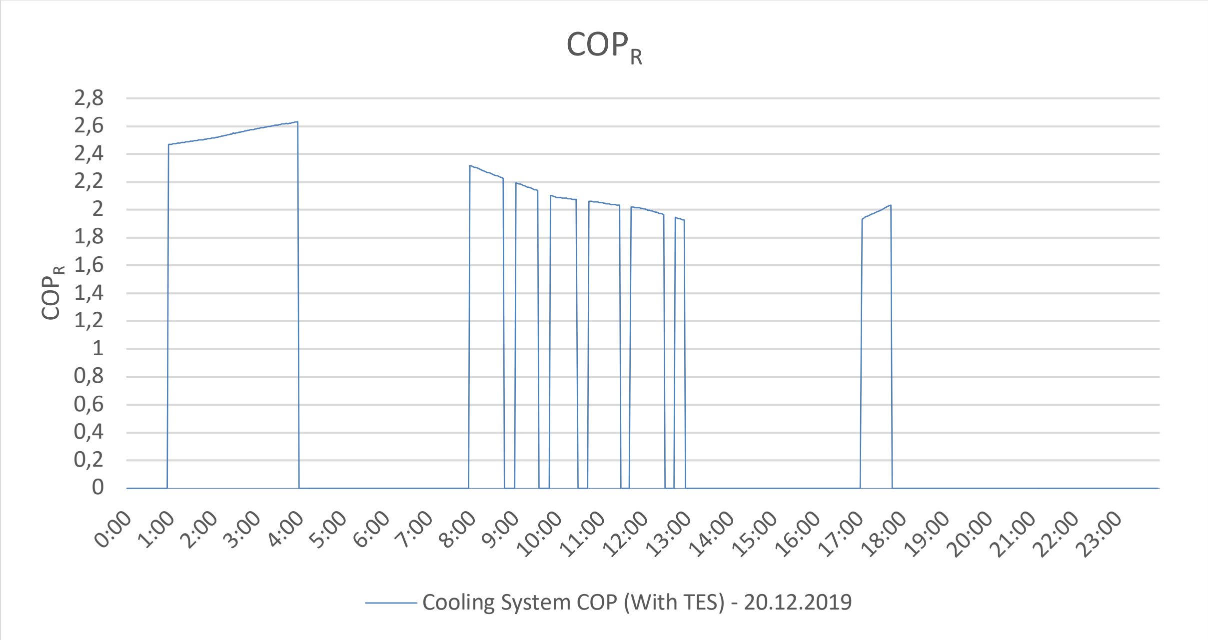

Source: Author

For 20.12.2019, an air conditioner with TES saves 10.6% in electricity consumption, as shown in **Figure 31**.

Figure 31 – Power Consumption – 20.12.2019

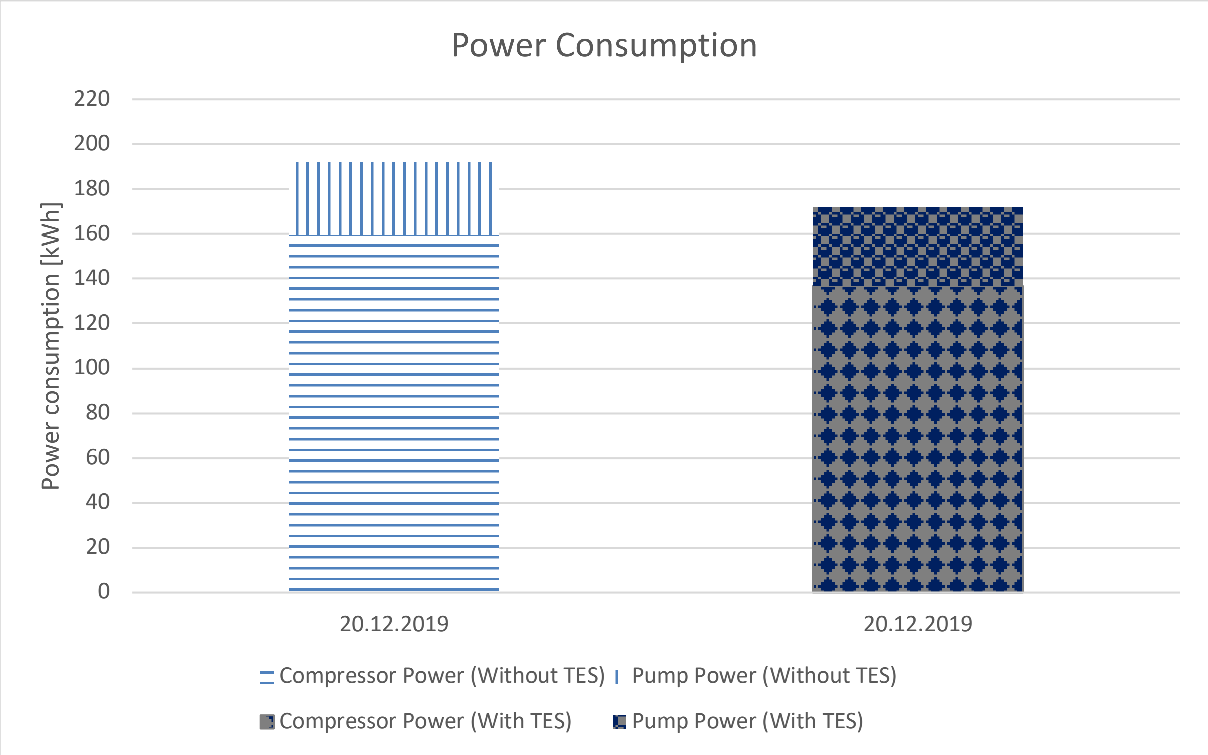

Source: Author

The lowest maximum temperature was recorded on 17.05.2019. **Figure 32** shows the external and internal temperatures of the simulated environment. For this day, the number of cycles of the air conditioning system was higher than on 20.12.2019, when the external temperatures and radiation rates were lower, as shown in **Figure 33**, and the thermal load of the simulated environment was also lower.

As a result of the lower external temperatures, the efficiency of the operation of the air conditioning system on 17.05.2019 was better than the other days presented, as can be seen in **Figure 34** and **Figure 35**, where the COP_R values are shown. The maximum COP_R presented during the charging period was 2.65, and the maximum value during the day was 2.7, and it was achieved during the business hour, where the COP_R values are shown. On this lower temperature day, the charging time was reduced by one hour when compared to 23.01.2019 and 20.12.2019; because of this shorter charging period, the stored heat was not sufficient to supply the entire discharge time, then the COP_R reappeared at the end of the business hour, showing that the air conditioning system must work again.

Figure 32 – Temperature – 17.05.2019

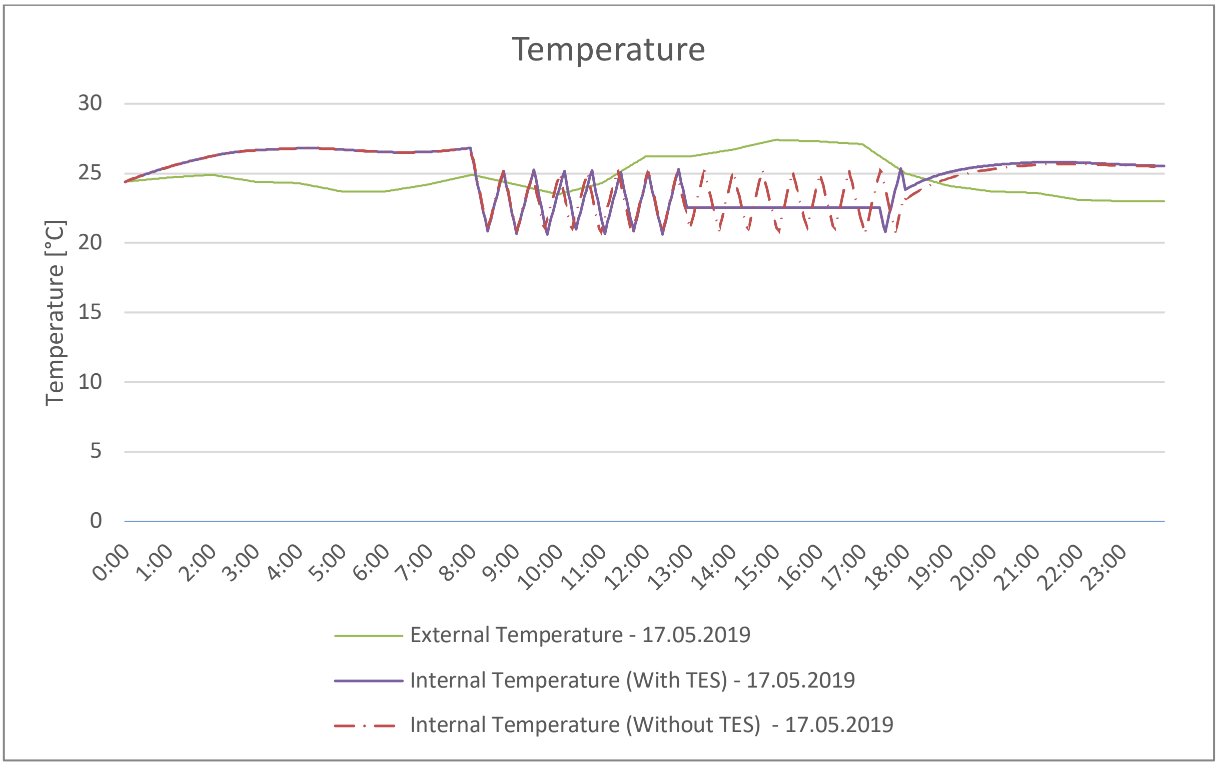

Source: Author

Figure 33 – Radiation – 17.05.2019

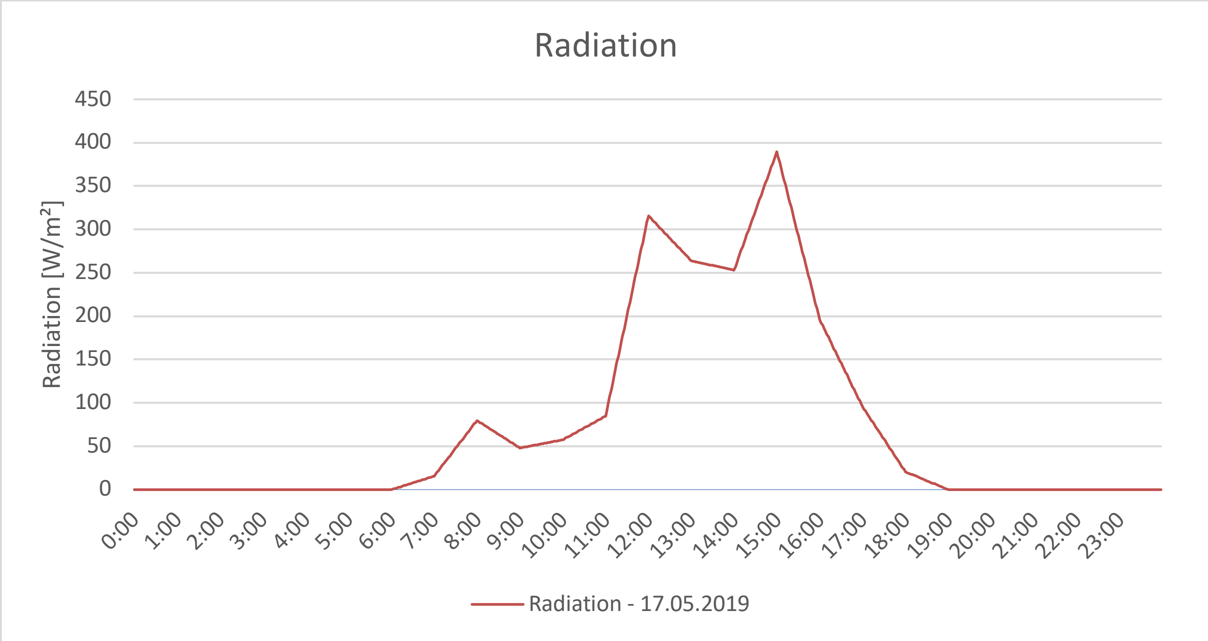

Source: Author

Figure 34 - System without TES - COP – 17.05.2019

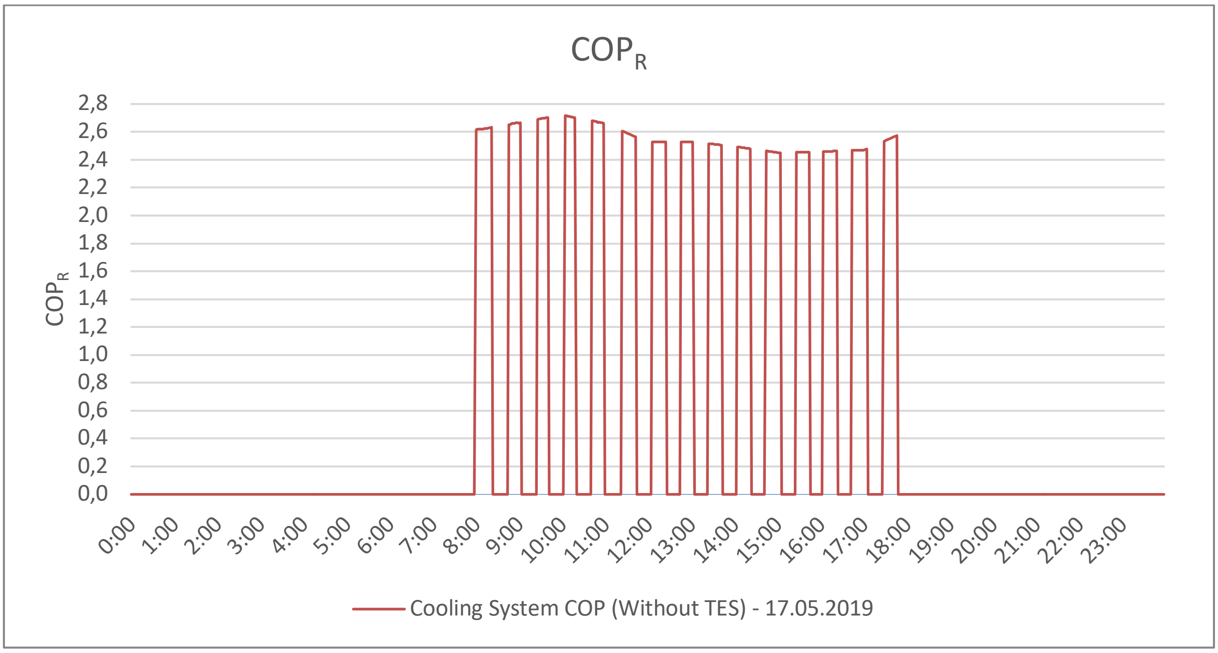

Source: Author

Figure 35 - System with TES - COP – 17.05.2019

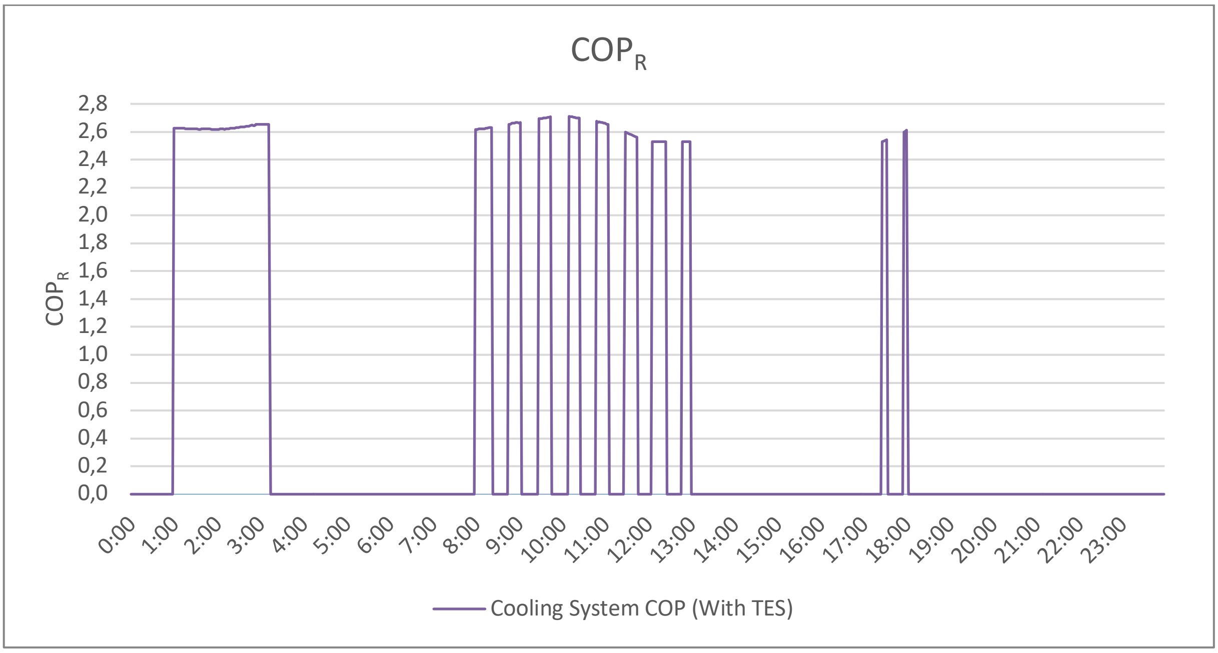

Source: Author

As a result of the short charging period, the solid fraction of the PCM is smaller, and the amount of heat was insufficient until the end of the discharge period, as shown in **Figure 36**. The amount of heat stored was less than the thermal load during the discharge period, as shown in **Figure 37**. The discharge time was sufficient to melt the PCM mass, as shown in **Figure 38**.

Figure 36 – PCM solid fraction – 17.05.2019

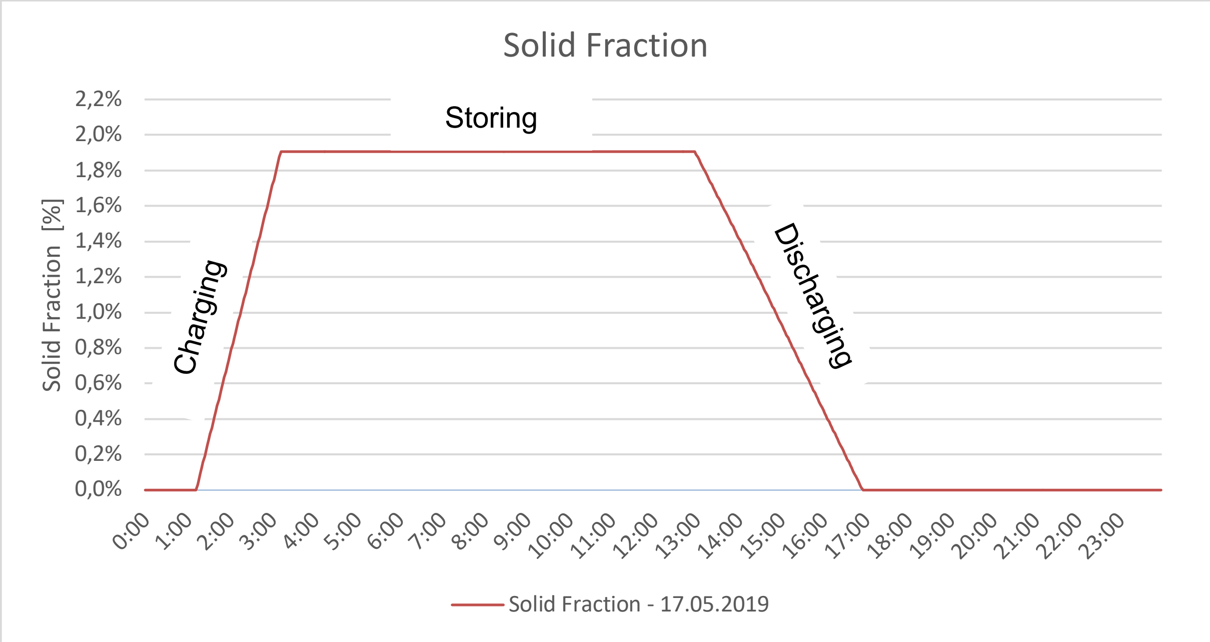

Source: Author

Figure 37 – PCM stored heat – 17.05.2019

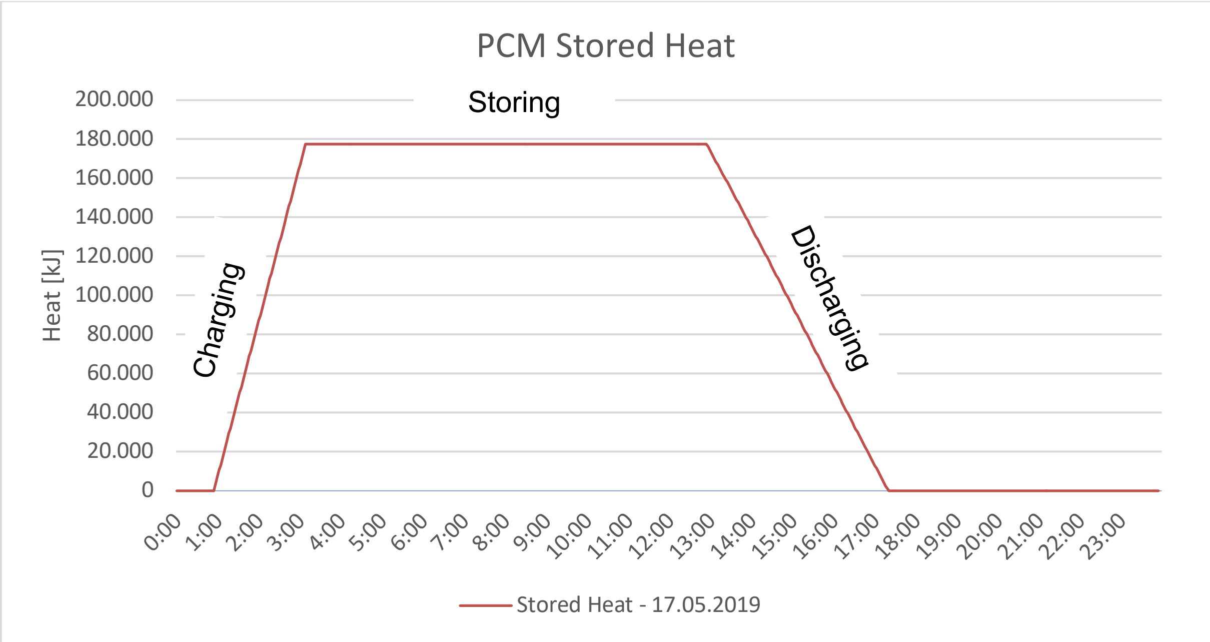

Source: Author

Figure 38 – PCM temperature – 17.05.2019

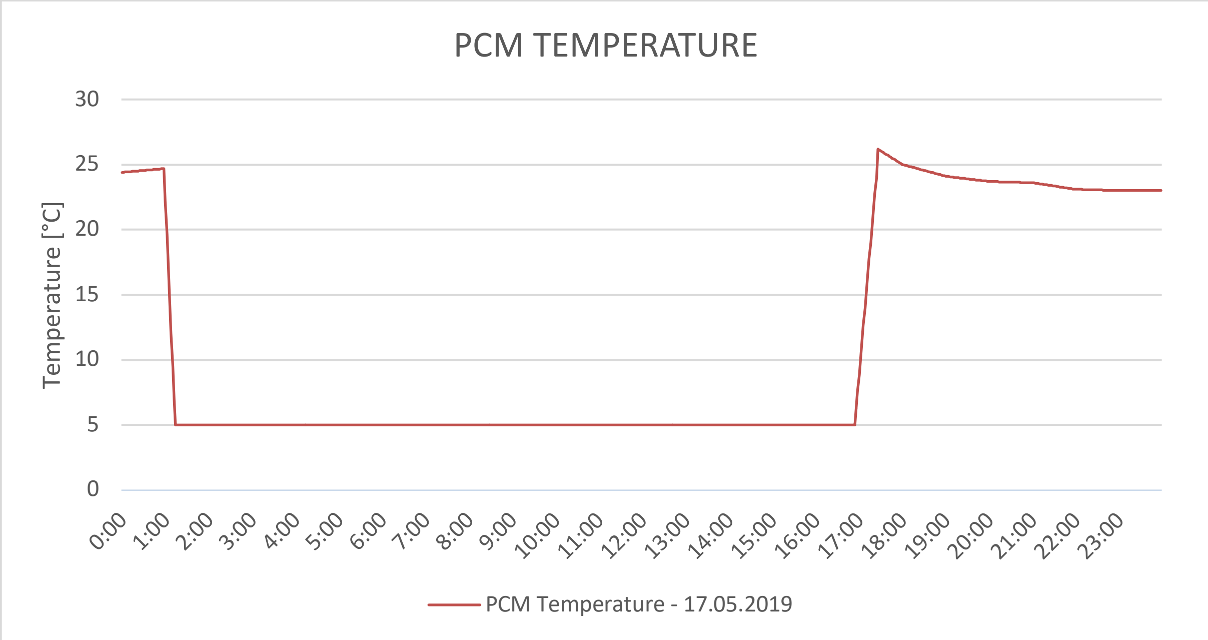

Source: Author

For 17.05.2019, an air conditioner with TES saves 1.3% in power consumption, as shown in **Figure 39**.

Figure 39 – Power Consumption – 17.05.2019

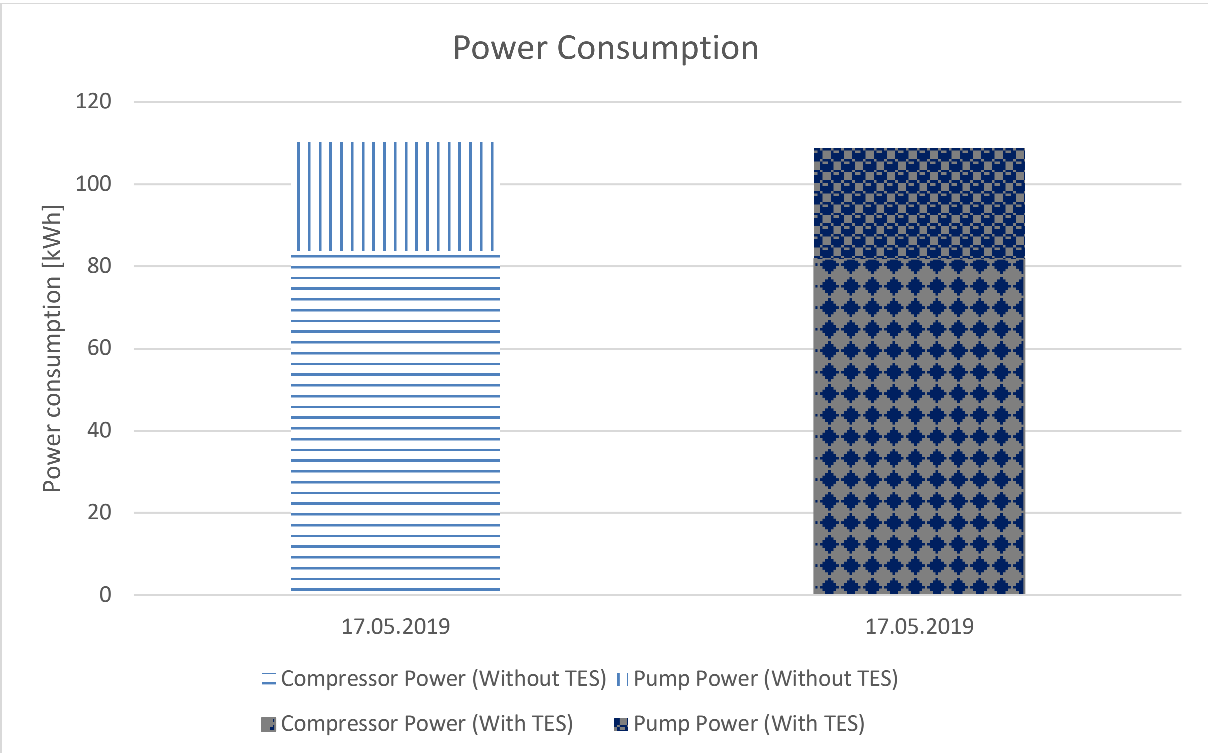

Source: Author

Considering the results presented above, we have that the highest COP_R value during the TES charging period was 2.65, observed on 17.05.2019, and the lowest was 2.55, observed on 23.01.2019. Therefore, we do not have a large variation during the year. The highest COP_R value during the TES discharge was 2.58 on 17.05.2019, and the lowest value was 2.07 on 23.12.2019. During the TES discharge period, the COP_R values show a greater variation than during the charging period. Considering the energy consumption reduction values presented, the air conditioning system coupled to the TES showed an average reduction of 4.8% in electrical energy consumption for air conditioning.

5 CONCLUSIONS

This master's thesis presents a mathematical model of the air conditioning system integrated with thermal energy storage using phase change material. The developed mathematical model was able to determine the thermal loads and the temperature of the simulated environment, and with that information, it was possible to simulate the air conditioning system working to control the internal temperature during business hours.

An air-cooled chiller operating in Teresina – PI / Brazil is used to meet the thermal load. Three days of the year were chosen: the day with the maximum sum of solar radiation and the day with the minimum and maximum air temperature.

The simulation results show that the air conditioning system with TES saves 9.4% of energy on the hottest day, 3.8% on the day of the highest incidence of solar radiation, and 1.3% on the day of the lowest maximum temperature.

REFERENCES

ABEDIN, A. H.; ROSEN, M. A. A Critical Review of Thermochemical Energy Storage Systems. **The Open Renewable Energy Journal**, v. 4, p. 42-46, May 2011. ISSN 905/7213370.

AJAROSTAGHI, S. S. M. et al. Numerical Modeling of the Melting Process in a Shell and Coil Tube Ice Storage System for Air-Conditioning Application. **Applied Sciences**, v. 9, n. 13, p. 2726, July 2019. ISSN 2076-3417.

AKEIBER, H. et al. A review on phase change material (PCM) for sustainable passive cooling in building envelopes. **Renewable and Sustainable Energy Reviews**, v. 60, p. 1470-1497, 2016.

AL-ABIDI, A. A. et al. Experimental study of PCM melting in triplex tube thermal energy storage for liquid desiccant air conditioning system. **Energy and Buildings**, v. 60, p. 270–279, January 2013. ISSN http://dx.doi.org/10.1016/j.enbuild.2013.01.031.

ALJEHANI, A. et al. Design and optimization of a hybrid air conditioning system with thermal energy storage using phase change composite. **Energy Conversion and Management**, v. 169, p. 404–418, 2018.

ALJEHANI, A.; NITSCHE, L. C.; AL-HALLAJ, S. Numerical modeling of transient heat transfer in a phase change composite thermal energy storage (PCC-TES) system for air conditioning applications. **Applied Thermal Engineering**, v. 164, October 2020. ISSN 13594311.

ALLOUCHE, Y. et al. Experimental determination of the heat transfer and cold storage characteristics of a microencapsulated phase change material in a horizontal tank. **Energy Conversion and Management**, v. 94, p. 275-285, February 2015. ISSN http://dx.doi.org/10.1016/j.enconman.2015.01.064.

ASSOCIAÇÃO BRASILEIRA DE NORMAS TÉCNICAS. **NBR 15220-1: Desempenho térmico de edificações. Parte 1: Definições, símbolos e unidades**. ABNT. Rio de Janeiro. 2005.

ASSOCIAÇÃO BRASILEIRA DE NORMAS TÉCNICAS. **NBR 15220-2: Desempenho térmico de edificações. Parte 2: Métodos de cálculo da transmitância térmica, da capacidade térmica, do atraso térmico e do fator solar de elementos e componentes de edificações**. ABNT. Rio de Janeiro. 2005.

ASSOCIAÇÃO BRASILEIRA DE NORMAS TÉCNICAS. **NBR 15220-3: Desempenho térmico de edificações Parte 3: Zoneamento bioclimático brasileiro e diretrizes construtivas para habitações unifamiliares de interesse social**. ABNT. Rio de Janeiro. 2005.

ASSOCIAÇÃO BRASILEIRA DE NORMAS TÉCNICAS. **NBR 16401-1: Instalações de ar-condicionado—Sistemas centrais e unitários. Parte 1: Projetos das Instalações**. ABNT. Rio de Janeiro. 2008.

BAETENS, R.; JELLE, B. P.; GUSTAVSEN, A. Phase change materials for building applications: A state-of-the-art review. **Energy and Buildings**, v. 42, p. 1361–1368, March 2010. ISSN doi:10.1016/j.enbuild.2010.03.026.

CHAIYAT, N. Energy and economic analysis of a building air-conditioner with a phase change material (PCM). **Energy Conversion and Management**, v. 94, p. 150-158, February 2015. ISSN ISSN 0196-8904.

CHEN, W. et al. Investigation on the thermal performance and optimization of a heat pump water heater assisted by shower waste water, 64, September 2013. 172-181.

DE PAULA, C. H. et al. Energetic, Exergetic, Environmental, and Economic Assessment of a Cascade Refrigeration System Operating with Four Different Ecological Refrigerant Pairs. **International Journal of Air-Conditioning and Refrigeration**, 2021.

DUARTE, W. et al. FEASIBILITY OF THERMAL STORAGE FOR AIR CONDITIONER: A CASE OF STUDY FOR OFFICE APPLICATIONS. **Brazilian Congress of Thermal Sciences and Engineering**, n. 18th, November 2020.

DUARTE, W. M. et al. Refrigerants selection for a direct expansion solar assisted heat pump for domestic hot water. **Solar Energy**, 184, April 2019. 527–538.

DUARTE, W. M. et al. Comparative study of geothermal and conventional air conditioner: a case of study for office applications. **18th Brazilian Congress of Thermal Sciences and Engineering. ENCIT**, 2020b.

DUTRA, C. G. D. O.; DUARTE, W. M.; PAULINO, T. D. F. The Brazilian Perspective Of Thermal Energy Storage Focused On Air Conditioning And Water Heating For Bath: Literature Review. **Brazilian Congress of Thermal Sciences and Engineering**, 2020.

EAMES, I. W.; MILAZZO, A.; MAIDMENT, G. G. Modelling thermostatic expansion valves. **International Journal of Refrigeration**, v. 38, p. 189-197, February 2014. ISSN ISSN 0140-7007.

EPE. NOTA TÉCNICA EPE 030/2018. Uso de Ar Condicionado no Setor Residencial Brasileiro: Perspectivas e contribuições para o avanço em eficiência energética. **Ministério de Minas e Energia**, 2018.

FANG, G.; LIU, X.; WU, S. Experimental investigation on performance of ice storage air-conditioning system with separate heat pipe. **Experimental Thermal and Fluid Science**, v. 33, p. 1149–1155, July 2009. ISSN doi:10.1016/j.expthermflusci.2009.07.004.

FASL, J. M. et al. Dynamic Model of a Refrigeration System with Active Thermal Energy Storage. **ASHRAE Transactions**, v. 120, n. 1, 2014.

FERREIRA, D. M. et al. CÁLCULO SIMPLIFICADO DE CARGA TÉRMICA EM EDIFICAÇÕES. **XXII Congresso Nacional de Engenharia Mecânica e Industrial**, São Paulo, Outubro 2022.

GNIELINSKI, V. New equations for heat and mass transfer in turbulent pipe and channel flow. **Int. Chem. Eng**, 2, n. 16, 1976. 359 - 368.

HUGHMARK, G. A. An improved void fraction model for two-phase cross-flow in horizontal tube bundless. **Chem. Eng. Prog.**, 58, 1962. 62 – 65.

IEA. **World Energy Balances: Overview**. IEA. Paris. 2021.

INCROPERA, F. P. et al. **Fundamentals of heat and mass transfer**. New York : John Wiley & Sons, 2011.

KONG, X. Q. et al. Modeling evaluation of a direct-expansion solar-assisted heat pump water heater using R410A. **International Journal of Refrigeration**, 76, 2017. 136-146. Disponivel em: <https://doi.org/10.1016/j.ijrefrig.2017.01.020>.

KOSMADAKIS, G. et al. Techno-economic analysis of high-temperature heat pumps with low-global warming potential refrigerants for upgrading waste heat up to 150°C. **Energy Conversion and Management**, 226, 2020.

KUTLU, C. et al. Direct-expansion solar-assisted heat pump coupled with crystallisation controllable supercooled PCM for shifting the building electricity demand. **Energy & Buildings**, 17 October 2023.

LI, S.-F.; LIU, Z.-H.; WANG, X.-J. A comprehensive review on positive cold energy storage technologies and applications in air conditioning with phase change materials. **Applied Energy**, v. 255, p. 113667, 2019.

LI, X.-Y. et al. Investigation on the charging process of a multi-PCM latent heat thermal energy storage unit for use in conventional air-conditioning systems. **Energy**, v. 150, p. 591-600, March 2018. ISSN https://doi.org/10.1016/j.energy.2018.02.107.

LIN, Y. et al. Performance investigation on an air source heat pump system with latent heat thermal energy storage. **Energy**, v. 239, p. 121898, September 2021. ISSN https://doi.org/10.1016/j.energy.2021.121898.

LIU, J.; TIAN, X.; LIN, Z. Performance analysis of a novel dual heat source warm air heating system with ecofriendly refrigerants. **Building and Environment**, 194, February 2021.

LOEM, S. et al. Study on phase change material thermal characteristics during air charging/discharging for energy saving of air-conditioner. **Heat and Mass Transfer**, v. 56, n. 7, p. 2121-2133, February 2020.

MAKHNATCH, P.; KHODABANDEH, R. The role of environmental metrics (GWP, TEWI, LCCP) in the selection of low GWP refrigerant. **Energy Procedia**, 61, 2014. 2460 - 2463.

METTAWEE, E. B. S.; EID, E. I.; AMIN, S. A. M. Experimental Study on Space Cooling with PCM Thermal Storage. **Journal of Applied Sciences Research**, v. 8, n. 7, p. 3424-3432, 2012.

MINETTO, S. Theoretical and experimental analysis of a CO2 heat pump for domestic hot water. **International Journal of Refrigeration**, 34, 2011. 742-751. Disponivel em: <https://doi.org/10.1016/j.ijrefrig.2010.12.018>.

MORENO, P. et al. PCM thermal energy storage tanks in heat pump system for space cooling. **Energy and Buildings**, v. 82, p. 399–405, July 2014.

NIE, B. et al. Performance enhancement of a phase-change-material based thermal energy storage device for air-conditioning applications. **Energy and Buildings**, v. 214, p. 109895, May 2020. ISSN ISSN 0378-7788.

NKWETTA, D. N.; HAGHIGHAT, F. Thermal energy storage with phase change material - A state-of-the art review. **Sustainable Cities and Society**, v. 10, p. 87-100, 2014. ISSN 22106707.

OSTERMAN, E. et al. Parametrical analysis of latent heat and cold storage for heating and cooling of rooms. **Applied Thermal Engineering**, v. 84, p. 138e149, March 2015. ISSN http://dx.doi.org/10.1016/j.applthermaleng.2015.02.081.

PALACIO, S. N. et al. Reducing power system costs with thermal energy storage. **Applied Energy**, v. 129, p. 228–237, April 2014. ISSN 03062619.

PARDIÑAS, Á. Á. et al. State-of-the-Art for the use of Phase-Change Materials in Tanks Coupled with Heat Pumps. **Energy and Buildings**, January 2017. ISSN DOI: http://dx.doi.org/doi:10.1016/j.enbuild.2017.01.061.

PROCEL. Pesquisa de posse de equipamentos e hábitos de uso: Setor comercial. Ano base: 2005. **PROCEL ELETROBRÁS**, 2008.

QV, D. et al. Reliability verification of a solar–air source heat pump system with PCM energy storage in operating strategy transition. **Renewable Energy**, v. 84, p. 46-55, July 2015. ISSN http://dx.doi.org/10.1016/j.renene.2015.07.030.

RAHDAR, M. H.; EMAMZADEH, A.; ATAEI, A. A comparative study on PCM and ice thermal energy storage tank for air-conditioning systems in office buildings. **Applied Thermal Engineering**, v. 96, p. 391–399, 2016. ISSN http://dx.doi.org/10.1016/j.applthermaleng.2015.11.107.

REAL, A. et al. Improvement of a heat pump based HVAC system with PCM thermal storage for cold accumulation and heat dissipation. **Energy and Buildings**, v. 83, p. 108–116, April 2014. ISSN http://dx.doi.org/10.1016/j.enbuild.2014.04.029.

REAL-FERNÁNDEZ, A. et al. Modeling of a PCM TES tank used as an alternative heat sink for a water chiller. Analysis of performance and energy savings. **Energies**, v. 19, dez. 2019. ISSN 10.3390/en12193652.

SAID, M. A.; HASSAN, H. Parametric study on the effect of using cold thermal storage energy of phase change material on the performance of air-conditioning unit. **Applied Energy**, v. 230, p. 1380-1402, September 2018. ISSN ISSN 0306-2619.

SAID, M. A.; HASSAN, H. A study on the thermal energy storage of different phase change materials incorporated with the condenser of air-conditioning unit and their effect on the unit performance. **Energy & Buildings**, v. 202, August 2019. ISSN ISSN 0378-7788.

SANTOS, A. H. C. et al. REFRIGERANT SELECTION FOR A CHILLER AIR CONDITIONING SYSTEM IN BRAZIL. **19th Brazilian Congress of Thermal Sciences and Engineering**, Bento Gonçalves, November 2022.

SARBU, I.; SEBARCHIEVICI,. A Comprehensive Review of Thermal Energy Storage. **Sustainability**, v. 10, n. 191, January 2018.

SHAH, M. M. Comprehensive correlations for heat transfer during condensation in conventional and mini/micro channels in all orientations. **International Journal of Refrigeration**, 67, July 2016. 22-41.

SHAH, M. M. Unified correlation for heat transfer during boiling in plain mini/micro and conventional channels. **International Journal of Refrigeration**, 74, 2017. 606–626.

SOCACIU, L. G. Thermal energy storage with phase change material. **Leonardo Electronic Journal of Practices and Technologies**, v. 11, n. 20, p. 75-98, August 2012. ISSN 1583-1078.

UNFCCC. **Adoption of the Paris Agreement**. Bonn, Germany: [s.n.]. 2015.

UNFCCC. **Kyoto Protocol to the United Nations Framework Convention on Climate Change**. Proceedings of the Third Session of the Conference of the Parties (COP3). Kyoto, Japan,: [s.n.]. December 1997.

VEERAKUMAR, C.; SREEKUMAR, A. Phase change material based cold thermal energy storage: Materials, techniques and applications - A review. **International Journal of Refrigeration**, n. 67, p. 271-289, 2016. ISSN 01407007.

XIA, Y. et al. Emerging Applications of Phase-Change Materials (PCMs): Teaching an Old Dog New Tricks. **Angewandte Reviews**, v. 53, p. 3780 - 3795, 2014. ISSN DOI: 10.1002/anie.201305201.

XIAO, X.; ZHANG, P. Numerical and experimental study of heat transfer characteristics of a shell-tube latent heat storage system: Part I - Charging process. **Energy**, v. 79, p. 337-350, 2015.

ZHANG, D. et al. Effects of refrigerant charge and structural parameters on the performance of a direct-expansion solar-assisted heat pump system. **Applied Thermal Engineering**, v. 73, n. 1, p. 522-528, December 2014. ISSN https://doi.org/10.1016/j.applthermaleng.2014.07.077.

ZHANG, N.; LI, Y.; DING, Z. Investigation on the energy performance of using air-source heat pump to charge PCM storage tank. **The Journal of Energy Storage**, v. 28, April 2020. ISSN 2352-152X.

ZHAO, D.; TAN, G. Numerical analysis of a shell-and-tube latent heat storage unit with fins for air-coditioning application. **Applied Energy**, v. 138, p. 381–392, November 2015. ISSN 0306-2619.

ZHENG, L. et al. Experimental study on the thermal performance of solar air conditioning system with MEPCM cooling storage. **International Journal of Low-Carbon Technologies**, v. 14, p. 83–88, 2019.

ZUKAUSKAS, A. Heat transfer from a single tubes and banks of tubes in crossflow. **Advances in Heat Transfer**, 8, 1972. 843-865.

ANNEX I - Papers

This master's thesis is the result of research carried out under the guidance of Prof. Doctor Tiago Freitas Paulino from Centro Federal de Educação Tecnológica de Minas Gerais – CEFET-MG and Prof. Doctor William Moreira Duarte from Universidade Federal de Minas Gerais – UFMG. During that time, two conference/congress papers related to this research were produced and are listed below:

FERREIRA, D. M. et al. CÁLCULO SIMPLIFICADO DE CARGA TÉRMICA EM EDIFICAÇÕES. **XXII Congresso Nacional de Engenharia Mecânica e Industrial**, São Paulo, Outubro 2022.

SANTOS, A. H. C. et al. REFRIGERANT SELECTION FOR A CHILLER AIR CONDITIONING SYSTEM IN BRAZIL. **19th Brazilian Congress of Thermal Sciences and Engineering**, Bento Gonçalves, November 2022.

SANTOS, A. H. C.; PAULINO, T. F.; DUARTE, W. M.; BARBIERI, P. E. L.; Air Conditioning System integrated with Thermal Energy Storage for buildings. Submitted to **Applied Energy**. Under review.